Chapter 3
Changes in the Structural-Phase State of Ferrite-Perlite Steel Under the Action of Electrolyte-Plasma Surface Quenching: Electrolytic-Plasma Surface Quenching of Steel Grade Two

Yerkezhan Tabiyeva
https://orcid.org/0000-0002-9726-7187
D. Serikbayev East Kazakhstan Technical University, Kazakhstan

Didar Yeskermessov
https://orcid.org/0000-0002-2206-8132
D. Serikbayev East Kazakhstan Technical University, Kazakhstan

Bauyrzhan Rakhadilov
PlasmaScience LLP, Kazakhstan

Zarina Aringozhina
https://orcid.org/0009-0001-8428-4033
D. Serikbayev East Kazakhstan Technical University, Kazakhstan

Gulzhaz Uazyrkhanova
D. Serikbayev East Kazakhstan Technical University, Kazakhstan

Waqar Ahmed
University of Lincoln, UK

ABSTRACT

This chapter presents an analytical review of literature sources devoted to research on the rapid heating of steels using various heat sources; in particular, on plasma surface hardening of materials. The results of studying the effect of a hardened surface layer during plasma hardening in the cathodic mode on the mechanical and tribological characteristics of grade two wheel steel are presented. Based on the experimental data obtained, a method for electrolytic-plasma surface hardening of wheel steel was developed and the optimal mode was determined. A description of the phase composition and morphology of grade two steel in the initial state and after electrolytic-plasma surface hardening is given. These descriptions are accompanied by images obtained by transmission electron microscopy. The authors present bright-field images and microdiffraction patterns obtained from these areas, as well as their dark-field patterns.

DOI: 10.4018/978-1-6684-6830-2.ch003

INTRODUCTION

The development of modern mechanical engineering is associated with the development of new materials, the introduction of new technologies and equipment, the invention of new ways to improve the performance of machine parts and mechanisms. The wear resistance, strength and corrosion resistance of machine parts are significantly affected by the condition of their surface layer, which is dictated by the manufacturing technology. Because the destruction of the surface during wear leads to the failure of 60-80 percent of mechanical engineering products (Makarov, 2009). Wear of working surfaces and fatigue of joints are key factors limiting the strength and reliability of various components of railway transport, construction, road and agricultural machinery, metallurgical and pressing equipment. Wear leads to a change in the shape, size and condition of the surface of the parts, which leads to a loss of functional qualities and operability of technical means of production, as well as to an increase in the probability of failure. Most mechanical engineering products are still made of steel or cast iron. Therefore, increasing the wear resistance of iron alloys is one of the most important and urgent tasks of technical physics.

There are several technical solutions to improve the quality of component surfaces. The most common electroplating and chemical methods of coating, surfacing, spraying, chemical and thermal treatment, surface hardening with high frequency currents, surface hardening with concentrated energy flows (plasma, electron beam, laser), etc. (Vyacheslav, 2018). Surface hardening by focused energy flows is the most promising method of surface hardening of iron alloys. However, the widespread introduction of some methods of surface hardening with a concentrated flow of energy, such as laser and electron beam, is hindered by the high cost and complexity of the equipment, its insufficient reliability and performance, the need for vacuum, special rooms with special requirements, the need for qualified maintenance and high operating costs (Lahtin & Arzamasov, 1985). As a consequence, according to its technical and economic indicators, as well as the results of a comparative study, a method of plasma surface hardening, devoid of the listed disadvantages, is proposed for widespread use (Troyannikov, 2021). Plasma surface hardening has been successfully developing in recent years and is currently widely used in various industries, primarily for the heat treatment of railway transport parts (the center plates of the freight wagons, the spring beam and the side frame of the trolley, the bandage, etc.) (Dyachenko, 1981).

Being one of the varieties of plasma quenching – electrolyte-plasma surface quenching (EPSQ) has recently been developing and intensively studied. This method is characterized by lower energy consumption, simplicity of technological equipment and large size of the hardened zone (Zaides, 2020). This method has several advantages, including a sufficiently high performance and the possibility of quenching parts of a larger and more complex profile, and the degree of hardening is equivalent to plasma quenching. It is well known (Tyurin, 1999) that the resource of steel parts is determined by the indicators of their operational characteristics (starting from the chemical composition of the material and ending with the conditions in which one or more parts should be operated), most of which are directly dependent on the structural and phase state of the material. There are very few publications devoted to the study of structural-phase transitions in wheel steel during plasma surface quenching, and they do not sufficiently cover the problems of structure formation. At the same time, there is no data in the literature on the treatment of wheel steels by the method of electrolytic-plasma hardening, which requires additional experimental work to assess the prospects for the applicability of the method for strengthening wheelset bands.

In connection with the above, this work focuses on the development of a method for hardening wheel steel, as well as the study of the formation of the structure, phase composition and tribological properties of the hardened surface layer of grade two steel by quenching during electrolytic plasma surface treatment.

1. PLASMA SURFACE HARDENING OF MATERIALS

In this section are presented analytical review of literature sources devoted to research on high-speed heating of steels using various heat sources, in particular, on plasma surface hardening of materials, is presented. The results of studies of the experimental work carried out on surface hardening of the working surfaces of steel parts using various methods and technologies used during manufacture or during their operation are considered.

1.1 The Status of Existing Methods of Surface Heat Treatment of Steels

Currently, methods of surface hardening of materials by forming nanoscale phases in them are poorly understood, although they are very promising, especially when modifying surface layers by plasma quenching, since nanostructured states are achieved especially effectively at high heating rates and with a short exposure time to high temperatures. Studies aimed at establishing the regularities of the formation of the main types of structures in materials allow us to purposefully apply certain modes of surface hardening to ensure the necessary complex of operational properties, therefore they are relevant (Tyurin, 1999).

Solving the issues of increasing the reliability and durability of critical products operating under extreme conditions under variable contact, shock, static loads require the use of modern high-strength materials and structural solutions. It is also possible to provide the necessary parameters of the product by changing the state of the surface layer of steel. There are large number of traditional technological processes for processing (hardening) surfaces, which have their own characteristics, advantages and disadvantages, but in the last decade much attention has been paid to high-energy methods for improving the surface of steels and, despite numerous publications, the mechanisms of hardening of metals and alloys cannot be considered fully elucidated (Majorov, 2009). The development of promising technologies aimed at improving traditional and creating new methods of influencing the surface to give it the properties required by operating conditions is undoubtedly one of the urgent tasks of modern science and technology (Paulmier, et al., 2008). Traditional technologies of thermal and chemical-thermal treatment of machine parts and tools are designed for volumetric surface treatment and do not allow local treatment of rapidly wearing areas (Balanovskij, 2006).

Along with metallurgical methods and heat treatment in the conditions of manufacturing plants, local surface hardening of wear surfaces using various technologies used both during manufacture and during operation is also considered to increase the service life of parts. At the same time, plasma and magnetoplasma surface hardening are recommended for widespread implementation from all existing methods of hardening (gas-flame, high-frequency currents, plasma, electron beam and laser) according to their technical and economic indicators and the results of comparative analysis (Leshinskij et al., 1990).

However, plasma and magnetoplasmic surface hardening technologies require the use of special expensive equipment, the creation of special processing sites and are economically feasible only for mass, large-scale production. Along with the above methods, one of the promising ones is electrolyte-plasma surface hardening (EPSH), which is the most economical and productive method. This technology is

characterized by lower energy consumption, simplicity of technological equipment and large size of the hardened zone (Skakov et al., 2012). The advantages of the method are sufficiently high process productivity and the ability to harden parts of large mass and complex profile, and the degree of hardening is comparable to plasma hardening (Kondrat'ev et al., 2014). Functional qualities of steel parts, such as chemical composition and conditions of use, which are directly related to the structural and phase state of the part, are used to predict their service life (Grechneva, 1992).

The works devoted to the engineering of surface layers of wheel steel in the literature over the past few decades (since 1970) are few (Balanovskij, & Nesterenko, 1992; Sadovsky & Malyshev, 1984; Skripkin, et al., 1992; Van Gyui, 2015) and they do not fully cover the issues of structure formation. At the same time, despite the available amount of work on plasma quenching, the issue of electrolyte-plasma surface quenching in an aqueous electrolyte solution has not been sufficiently studied, and the quantitative characteristics of the fine structure of grade two ferritic-perlite class wheel steel have not been studied, which make this work relevant for use in the engineering, railway and manufacturing industries of our country. Currently, electrolyte-plasma technologies are intensively studied in many scientific and production teams, which indicates the relevance of research and the demand for their results by industry (Tyuftyaev, 2002).

Modern technologies of surface hardening of metals and alloys using concentrated energy flows (CEF), such as laser beam (Chudina, 2003; Majorov, 2009), electron beam (Poletika, et al., 2006), plasma arc (Balanovskij, 2015; Berdnikov, et al., ; Gulyaev, 1986), are characterized by high heating and cooling rates, short duration and locality of impact on the metal. The main requirements on the part of industrial enterprises when using new strengthening technologies based on CEF are associated with increasing the strength, wear and corrosion resistance of machine parts and tools (Zhang et al., 2009). The information available in the literature provides contradictory information about the prospects for the introduction of hardening technologies in various industries (Balanovskij, & Grechneva, 2015; Richard, 2007). Each of the authors of a particular technology gives a subjective assessment of the prospects of its development, finding shortcomings in other methods of hardening. In addition, the theory and practice of processing metals with concentrated energy flows are still far from perfect.

One of the first works on concentrated energy flows, in particular, on plasma surface hardening, were carried out at the Irkutsk Polytechnic Institute under the supervision of Professor V.N. Matkhanov. In the first works (Grigoriants, & Safonov, 1987; Lakhtin & Arzamasov, 1985; Zhang et al., 2005), the peculiarities of heating and cooling metals and alloys by concentrated energy flows were only stated without further investigation. Fundamentally new structures and phases in metals at extreme heating and cooling rates compared to furnace heat treatment, quenching with high frequency currents, welding were not detected. The resulting structures in the impact zone did not differ externally from the traditional ones observed in optical and electron microscopes (Balanovskij, 2016; Samotugin, et al., 1997), according to the authors, in general, everything looked consistent with the classical theory of phase and structural transformations.

At the same time, there was a high hardness and degree of dispersion of the resulting structures, heterogeneity of their distribution over the width and depth of the surface layer (Balanovskij, & Pletnikov, 1999; Balanovskij, & Pletnikov, 1999). In (Balanovskij, 2006; Stalinskij, & Rudyuk, 2007), new hypotheses of phase transformations were put forward from the perspective of nonequilibrium thermodynamics and the results of relevant experimental studies were presented, as well as an attempt was made to build a physical basis for the theory and practice of plasma surface hardening by the authors of the works. In (Medvedev, et al., 2015; Tyurin, 1999), general issues of plasma hardening were formulated for the

first time, research goals were set and tasks requiring solutions for the successful introduction of real plasma hardening technologies into production were outlined. In these works, an important fact is noted that the surface hardening of the CEF of metals is not a classical volumetric heat treatment with stable critical points Ac_1 and A_{C3}, the stage of homogenization, critical cooling rates, thermokinetic diagrams. The theoretical concepts adopted for the classical heat treatment of metals are used in the analysis of the processes of structure formation in the surface layer of metal only as a guide for research and further interpretation of the results (Balanovskii, 2016; Balanovskij, & Pletnikov, 1999).

Surface hardening of metals and alloys by concentrated energy flows is an interdisciplinary branch of scientific research that has, on the one hand, much in common with the main processes noted, and on the other hand, fundamental differences and patterns (Balanovskij, 2006). A number of works on plasma hardening are aimed at solving the technological problem of increasing the hardness of a particular steel grade from which a particular part is made (Pogrebnjak, & Tyurin, 2000; Skakov, Bayatanova, & Scheffler, 2013; Skakov, et al., 2012). Most of the research in this area has been carried out on equipment with fundamental design and technological features: plasma torches with interelectrode inserts (Tyuirin, & Pogrebnjak, 2001), different plasma–forming gases and media (Leshchinsky & Samotugin, 2001; Menin et al., 1981; Pogrebnjak, et al., 2003), different technological modes - a jet or an arc of direct or reverse polarity (Medvedovskaya & Shur, 1983; Polyak, 1995), a three-phase arc, a vacuum arc with different execution techniques, with magnetic or mechanical expansion of the jet (arc), a creeping or reflected plasma jet (Balanovskij, 2015; Balanovskij, 2016).

A separate area of work in the field of plasma hardening of metals and alloys is surface modification and alloying using plasma-forming media and elements. The use of liquid media as carriers of alloying elements in plasma surface hardening is considered in (Belkin, 2005). By conducting plasma hardening through a liquid medium, it is possible to saturate the surface layer with various alloying elements (nitrogen, carbon, boron, silicon, etc.), as well as reduce residual deformations and stresses. Plasma cyclic hardening is considered in (Tyurin, 2000), where studies are given on changes in the structure in the hardened layer depending on the number of heating cycles for carbon and alloy steels. The results of tests on the wear resistance of a large number of grades of steel and cast iron are presented. In this work, the mechanism of structure formation in the hardened layer is revealed in the process of multi-cycle heating and cooling, which contributes to obtaining structures of complete hardening in the hardened layer. The issue of structure formation during plasma hardening is considered in more detail in (Grechneva, 1992; Yerokhin, et al., 1999; Yushenko, et al., 1994) and the authors draw conclusions about the parameters of the technological process according to the final structure of the hardened layer.

In (Bayatanova, et al., 2012), the kinetics of austenite growth and cooling during plasma heating is considered and it is argued that the heating rate significantly affects the size of the austenitic grain: the higher the plasma heating rate, the smaller the size of the austenitic grain when heated, therefore, highly dispersed martensite is obtained during cooling. In this regard, the proposed technological thermograms make it possible to regulate the growth of austenite grains. The authors of (Kong et al., 2012), investigating the structure of hardened carbon steels after plasma quenching, fix a large amount of residual austenite in the hardened layer. In their opinion, this is due to the incompleteness of the hardening process. The results of the work show that cyclic treatment should be used to regulate the proportion of residual austenite (Balanovskij, 2016). Technologies of electron beam hardening of metals using carbon-containing pastes and coatings are widely used in industry (Korotkov, 2016). In contrast to this method, plasma surface hardening is possible both in the micro-melting mode of the surface (Ivanov, et al., 2011) and without it, which is unattainable for electron beam alloying methods. Visualization of

Figure 1. Comparison of martensite microstructures in a hardened layer of 080A67 steel a) with electronic quenching; b) laser and plasma quenching; c) in arc mode (the upper picture in the corner of the SEM, the general picture of the TEM)
Source: Grechneva (2017)

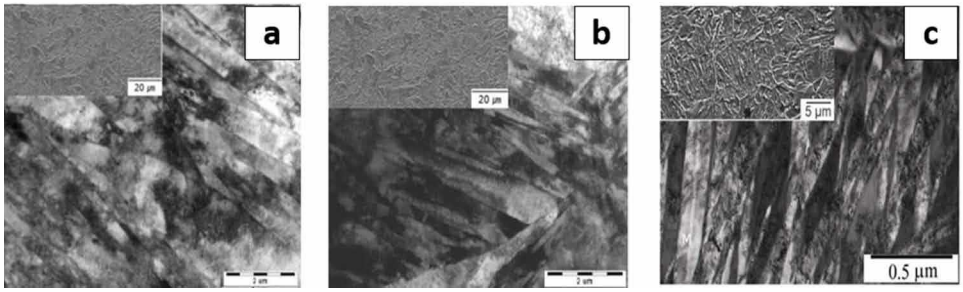

the plasma surface hardening process in the arc mode showed that for each steel grade there is a range of modes when surface melting does not occur (Balanovskij, 2016).

The presented information shows the competitiveness of the technology of plasma surface hardening of metals and alloys in comparison with other sources of concentrated energy. At the same time, the heterogeneity of technologies and equipment for plasma processing leads to different information about the processes of structure formation in the surface layer of metal. The results of a comparative evaluation of various methods of surface hardening summarized in (Grechneva, 2017) are shown in Figure 1.

The considered results of theoretical and experimental work in the field of plasma hardening represent the foundation for specific technologies of surface hardening of machine parts and tools. In particular, in the works (Korotkov et al., 1991), the issues of hardening of specific parts made of 5140, 1045, 080A67 steels are considered. For the first time, the effect of nanostructuring of the surface layer after plasma hardening was discovered during the development of plasma hardening technology for rail steel and was considered in detail in (Nesterov, & Sapozhkov, 1989). It is shown that the nanostructuring of the metal surface layer during plasma hardening depends on the modes used (Jin et al., 2013). In the works (Belkin, 2005; Kidin, 1978), new technological methods of heating machine parts and tools are proposed, which allow structuring the surface layer of metal at the nanoscale. In the development of this topic, a complex of works and studies has been carried out in order to develop a specific technology for plasma hardening of the bandage ridge (Tyuftyaev, 2002).

The results of the research carried out in the listed works with different types and technologies of surface hardening show the undeniable advantages of plasma surface hardening in comparison with the rest, both from the point of view of the economic component and from the side of resource conservation.

1.2 Physical Fundamentals of the Technology of Plasma Treatment of the Steel Surface in an Aqueous Electrolyte Solution

The development of scientific and technological progress in various spheres of the economy requires the widespread introduction into industry of new efficient and economical technological processes for strengthening materials based on the achievements of modern science and technology (Erkinbekkyzy et al.,). One of the promising areas that significantly expand the technological capabilities of the process of deep processing of metal products by strengthening heat treatment is the use of highly concentrated

energy flows (laser, plasma, electron beam, etc.). However, the widespread introduction of most of the known methods of hardening heat treatment with a highly concentrated energy flow, namely, laser, electron beam, cathode-ion, is constrained by the high cost and complexity of the equipment, its insufficient reliability and performance, the need to use vacuum, special rooms with special requirements, the need for qualified maintenance, high operating costs.

Unlike the processes listed above, the technology of surface electrolyte-plasma surface hardening of metals is devoid of the above disadvantages, has been successfully developing in recent years and is increasingly being used in various industries. Practice shows that surface plasma hardening is rational in terms of versatility, accessibility, environmental friendliness and economic efficiency in order to extend the operational life of heavily loaded parts and assemblies. Without changing the surface roughness parameters, such a hardening heat treatment is easily integrated into the technological process of restoring parts, is low-cost, sufficiently productive and allows to effectively increase their operational durability (Skakov, Kurbanbekov, Tabieva, et al, 2013). In the electrolyte-plasma technology, the processed product is an anode or cathode, a corresponding positive or negative potential from the power source is supplied to it, and the working bath serves as the opposite electrode. Depending on the applied voltage when an electric current passes through an aqueous electrolyte solution (Balanovskii, 2016).

The available experimental data indicate that the classical laws of electrochemistry are fulfilled only at low values of current and voltage densities on the electrodes (Moon, & Jeong, 2009). A more general physical picture is when, after exceeding the critical values of the electrical parameters, a gas-plasma cloud forms around the metal electrode, pushing the electrolyte away from the electrode surface. In this case, a multiphase metal–plasma–gas–electrolyte system arises, in which not only ions, but also electrons serve as charge carriers, and the phenomena occurring in the near-electrode region do not fit into the framework of classical electrochemistry. The passage of an electric current through an electrolyte cell containing two metal electrodes, one of which has a much smaller surface than the second, with a gradual increase in voltage at the electrodes leads to different phases or modes of the process, which can be traced to the volt-ampere characteristic of the active electrode–electrolyte system (Figure 2).

Figure 2. Volt-ampere characteristic of the active electrode-electrolyte system
Source: Kulikov et al. (2010)

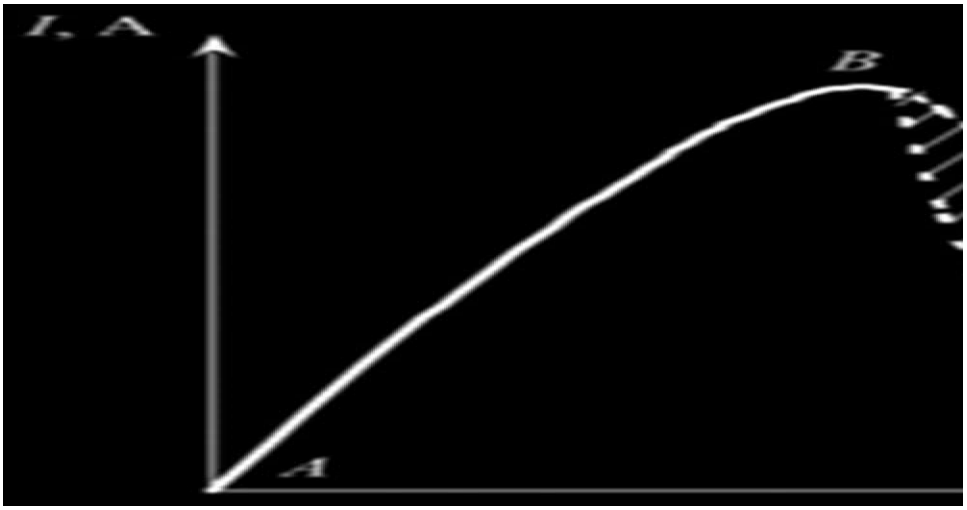

The AB section in Figure 2 is a conventional electrolysis process in which metal ions are transferred and gas release is observed depending on the composition of the electrolyte and the electrode material, and is described by classical electrochemistry. This section on the volt-ampere characteristic has a linear dependence of current on voltage, which means a constant value of the electrical resistance of the interelectrode gap.

With an increase in the voltage on the electrodes to 60-70 V, a transient or switching mode is established (a section of the BC), when a vapor-plasma shell is formed periodically around the active electrode, with a frequency of about 100 Hz, leading to current locking for 10^{-4} seconds (Kulikov et al., 2010). Due to the continuous change in the electrical resistance of the near-electrode region, each voltage value corresponds to a range of possible current values. At the moment of opening the circuit, a voltage pulse occurs according to the law of self-induction. The magnitude of the voltage in the switching mode may be variable. The resulting neutral gas shell periodically breaks through the resulting voltage pulse. After the breakdown, the active electrode comes into contact with the liquid electrolyte again and the process repeats. At a voltage of more than 200 V, the CD section indicated in Figure 2 forms a stable vapor-plasma shell around the active electrode, characterized by small current fluctuations at constant voltage. In this voltage region, the process of electrolyte-plasma treatment takes place. The falling character of the volt-ampere characteristic in this section can be considered as an increase in the resistance of the circuit with an increase in voltage. The increase in resistance is explained by an increase in the thickness of the vapor-gas shell. The solid vapor-plasma shell has a thickness of about 50 microns and constantly changes its shape. Electric current flows through a complex metal–plasma–gas–electrolyte system (Duradzhi & Parsadanyan, 1988).

With a further increase in voltage, the intensity of the glow of electric discharges increases, which leads to an increase in the thickness of the vapor plasma shell and separation over the entire surface of the active electrode, which is accompanied by a decrease in the current value by 2-2.5 times. An electrohydrodynamic mode is established in which the temperature of the active electrode drops to 100°C with and the effect of the vapor-plasma shell disappears. Studies have shown (Kulikov et al., 2010) that the onset of the electrohydrodynamic regime depends on the concentration of the electrolyte. With an increase in the concentration of the solution, this mode is set at a lower voltage.

The current density is the main parameter that must be controlled during the electrolytic plasma treatment (EPT) process. Usually, to achieve the necessary conditions for plasma electrolysis, the current density is set within 0.01–0.3 A/cm^2. According to Faraday's first law, this determines the growth rate of the coating. As the coating grows, the voltage increases rapidly at first, then slowly, until constant plasma conditions are established. The critical rate of voltage change corresponds to the establishment of a spark discharge on the surface of the electrode. This value is very dependent on the characteristics of the metal–electrolyte combination and is usually located in the range of 120-350 V. At the first stage of the process, sparking is observed in the form of uniform white light surrounding the electrode. As the coating grows, it changes and appears as individual yellow sparks that move rapidly through the surface. Gradually, the density of sparks decreases, but their power increases. Finally, several red spots appear, slowly moving through the surface. From time to time, these powerful arcs lead to current fluctuations and damage to the coating. Therefore, as soon as such arcs are detected, the process is immediately terminated. EPT can be carried out using both anodic and cathodic polarization of the product (Kulikov et al., 2010).

1.3 Structural-Phase Transformations of Ferrite-Pearlite Steels Under Plasma Surface Hardening

Despite the difference in the physical processes underlying a particular method of surface hardening of metals (plasma, laser, electron beam, etc.), a common feature is characteristic of all - phase and structural transformations occur on the working hardened metal surface (Dunleavy et al., 2009). Let's consider the main, general points of the theory of hardening of ferrite-pearlite steels. As is known, the strength characteristics of any types of steel depend on the properties of the structural components of this steel, in our case ferrite and perlite as the main component of the structure of wheel steels.

Ferrite, depending on the degree of its alloying with other elements such as silicon, manganese, phosphorus, may have a different degree of hardening. To date, it can be said that such non-carbide-forming elements as phosphorus, silicon and nickel are entirely part of ferrite, molybdenum and chromium are partially dissolved in ferrite, whereas manganese can completely dissolve in ferrite. The most hardening effect is associated with carbon dissolved in the α-Fe lattice. The strength of the structural component also depends on the grain size and the Hall-Petch dependence is determined:

$$\sigma T = \sigma i + Kd^{-1/2}, \quad (1)$$

Value: σ_i – in ferrite-perlite steels, it is characterized by the friction stress of the α-Fe lattice, solid-solution hardening, hardening due to the formation of perlite, deformation hardening, dispersion hardening. $K_d^{-1/2}$ – grain boundary hardening.

The effect of these parameters on the yield strength of ferritic-pearlite steels is linearly additive, so it can be summed up. For a deeper understanding of the processes occurring during structure formation, we further use primary designations such as ferrite and iron carbide (cementite) Fe_3C, which are the main components in wheel steels.

In the first approximation, the contribution of the lattice is $2 \cdot 10^{-4}G$, where G is the shear modulus. The contribution of the lattice can be estimated by the ratio:

$$G_{dis} = \alpha 1 \cdot M \cdot G \cdot b \cdot \rho v^{1/2}, \quad (2)$$

where:

α_1 – coefficient depending on the nature of the distribution and interaction of the dislocation;
M – numerical coefficient;
b – the Brugers vector ~ 0,25 nm;
ρ_v – the density of dislocations in the grain volume.

Transmission electron microscopy or X-ray diffraction analysis of the material under study is used to determine the density of lattice dislocations.

Iron carbide (cementite) has a complex rhombic lattice, the unit cell of which consists of 72 Fe atoms and 24 C atoms, with a tightly packed structure where iron atoms are located in the interstices by carbon atoms, which provides a good orientation and structural correspondence between Fe_3C and γ-Fe, the same lattice correspondence is observed for Fe_3C and α-Fe. When martensite disintegrates, cementite is easily generated in it, which is known to have a high hardness.

Figure 3. Diagram of the "iron-carbon" state

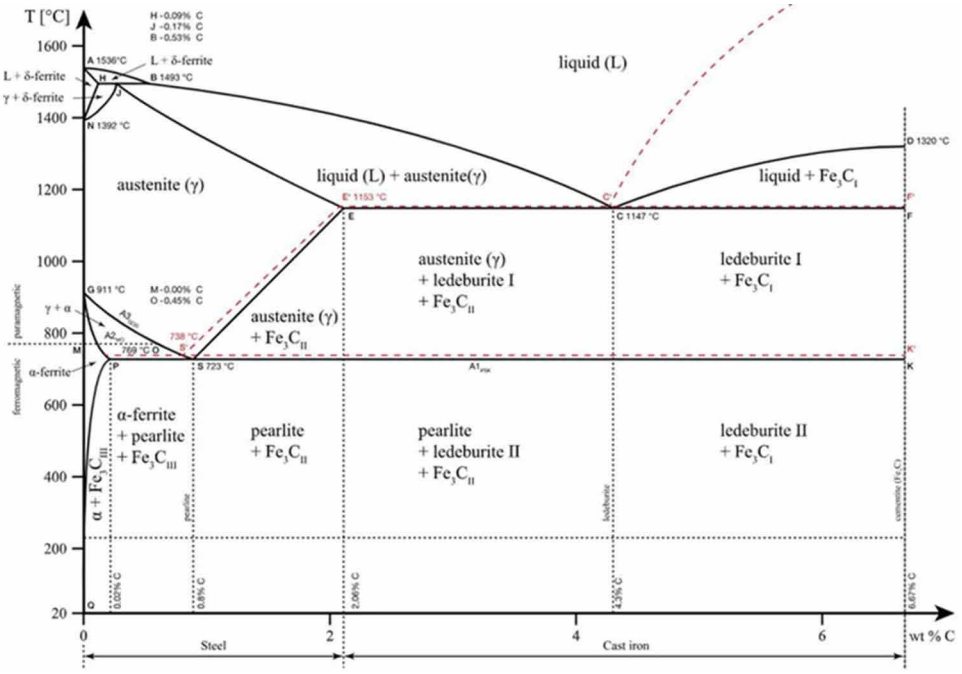

During the process of structuring, the iron atoms in cementite are easily replaced by atoms of some alloying elements that are part of the wheel steel. Thus, it was found that (Martin, et al., 2013), the basic element of wheel steel – manganese, is infinitely soluble in cementite, due to the fact that it forms a carbide similar to iron carbide. When analyzing the processes of structure formation during plasma hardening of wheel steel, it is important to take into account the structural properties of austenite formed in the high-temperature region in the "iron-carbon" transformation diagram (Figure 3).

Austenite, as a stable structure, exists at temperatures of 700-1400ⁱC (##NO_NAME##, 2012), and metastable in the form of residual austenite after quenching. It is this structure that, when cooled, forms the final structural components such as perlite, martensite, bainite, troostite. Thus, a preliminary analysis of previously available works on the theory of hardening applied to wheel steels shows that during plasma hardening, dislocation, dispersion and deformation hardening occupy the first rows, which depend on the cycle, the duration of heating and cooling of the surface layer, which ultimately determine the strength of the material. The plasma surface hardening process consists of the following stages: heating, phase transformation, partial homogenization and cooling. When surface quenching with melting of the surface, the melting process is turned on as another stage-melting. The main issues of austenite formation and the kinetics of grain growth under the influence of various parameters and factors affecting it were considered in detail in the works of S.Dyachenko (Dyachenko, 1981), V.Sadovsky, K.Malyshev (Sadovsky & Malyshev, 1984), A.Gulyaev (Gulyaev, 1986), and other authors. In the works of L.Leshchinsky, S.Samotugin, I.Pirch (Leshinskij et al., 1990) detailed comparative technical and economic assessments of various methods of surface hardening were carried out, which makes it possible not to consider this aspect in this study.

It is known (Wang et al., 2013) that the performance characteristics of steel parts vary from the chemical composition of the material to the conditions in which a particular part should be used, most of which directly depend on the structural and phase state of the part. Despite the available amount of work on plasma quenching, the issue of electrolyte-plasma surface quenching in an aqueous electrolyte solution has not been sufficiently studied, and the quantitative characteristics of the fine structure of grade two ferritic-pearlite grade wheel steel have not been studied, which make this work relevant for use in the engineering, railway and manufacturing industries of our country.

Conclusions on the Section

The analysis of the literature data shows that:

1. The combination of the existing classical technologies of heat treatment and surface hardening by local treatment of their working surface will allow to obtain high performance properties of steel products.
2. Electrolyte-plasma treatment is one of the promising methods tested by numerous authors of works on the modification of the structural-phase state of the surface layers of steels and alloys. This method is largely devoid of the disadvantages inherent in traditional mechanical and electrochemical processing methods, and additionally allows you to save material resources. Its advantages are high productivity and efficiency, compliance with environmental cleanliness, high quality and speed of operations performed. However, experimental data and information are not sufficient to conduct surface hardening of bandage steel in an aqueous electrolyte solution, as well as information about structural-phase transformations and features of the formation of a fine structure in the surface layers of grade two wheel steel during surface hardening in an aqueous electrolyte solution, which makes this study relevant.

2. MATERIAL AND METHODS OF RESEARCH

2.1 Research Material and Sample Preparation

In accordance with the tasks set, grade two bandage steel was chosen as the research material. This steel is carbon steel, used in the field of metallurgy and mechanical engineering, for the manufacture of bandages of freight, passenger and shunting locomotives, motor cars and diesel trains, subway cars and wheel bandages for pairs of tram cars. The chemical composition of grade two steel, according to GOST 398-96 is given in Table 1.

Table 1. Chemical composition, % (GOST 398-96)

Mass Fraction of Elements						
C	**Si**	**Mn**	**V**	**S**	**P**	**Fe**
0.57-0.65	0.22-0.45	0.60-0.90	no more			other
			0.15	0.04	0.035	
Note: according to GOST 398-96, it is allowed: Mo £ 0.08%, Ni £ 0.25, Cr £ 0.20%, Cu £ 0.30%.						

grade two steel in its initial state was a material that had been quenched from a temperature of 890°C (2-2.5 hours) with cooling in warm (30-60°C) water and subsequent tempering at 580°C (2.5-3 hours).

Blanks of steel samples of grade two for the study were cut out of a bandage in the form of a parallelepiped with a size of 15×15×10 mm^3. At low cutting speeds and low load, the sample does not experience deformation and thermal effects. Preparation of metallographic grinds of steel samples was carried out according to the methods.

2.2 Optical Metallography

Metallographic analysis is widely used in industry to control the structure of metal, semi-finished products and finished products to ensure their quality. To study the general nature of the structure, an optical microscope "ALTAMI-MET-1M" was used. The metallographic method of analysis has been introduced into a number of existing standards. According to the microstructure, the grain size was controlled [GOST 5639-82], the volume fraction of the material that has undergone decay and the volume fraction of the α-phase in grade two steel. The grain size of the microstructure of alloys was determined from photographs by the method of arbitrary secant, using the equation:

$$< d >= \frac{L \cdot p \cdot 10^3}{z \cdot B} \tag{3}$$

where:

L – secants length;
p – number of secants;
z – the number of grains crossed by straight lines;
B – magnification of the image in the photograph.

The slots for metallographic studies were prepared according to a standard technique, including mechanical grinding and mechanical polishing (Baranova, & Demina, 1986). Polishing was carried out on a grinding disc, covered with felt, pre-washed and soaked in water for 1-2 hours. Further, in order to identify the structure, the slots were etched. A 4% alcohol solution of nitric acid was used for etching. Qualitative and quantitative metallographic analysis was carried out according to the recommendations given in (Gorelik, et al., 2002; Rahadilov, 2014).

2.3 X-Ray Diffraction Analysis

Qualitative and quantitative phase analysis of the structure of steel samples was carried out on a Rengen diffractometer "X'pertPro" of the company "PANanalytical", using Cu-K_α radiation (λ=2.2897 A^0) at a voltage of 40 kV and a current of 30 mA. The samples were taken for reflection according to the Bragg–Brentano focusing scheme in cobalt and copper K_α - radiation. In order to exclude β-lines on diffractograms, a selectively absorbing β-filter made of iron was used when shooting on cobalt radiation, and a nickel filter was used when shooting on copper. When shooting on copper radiation, to exclude

the influence of fluorescent radiation on the diffraction pattern of the samples, an Aluminium foil with a thickness of 0.05 mm was used on the X'pertPro diffractometer. The decoding of diffractograms was carried out manually using standard techniques and the PDF-4 database, and quantitative analysis was performed using the Powder Cell program.

Sample preparation, selection of shooting modes and calculation of diffractograms were carried out according to the methods. The interplane distances d_i were determined from the Wulf-Bragg formula:

$$\frac{d_i}{n} d_{HKL} = \frac{\lambda}{2\sin\theta} \tag{4}$$

where:

λ – the wavelength of the characteristic X-ray radiation;
n – the order of reflection;
θ – diffraction angle.

The interference indices and the type of crystal lattice of the phases were determined by the series Q found for each phase from the expression:

$$Q = \sin^2\theta i / \sin 2^\theta 1 \tag{5}$$

According to the found HKL indices and the value of the interplane distance for the line in the area of angles 77-112°, the periods of the unit cell of the lattices present in the sample phases were determined from the ratio:

$$a = \frac{\lambda}{2\sin\theta} \cdot \sqrt{H^2 + K^2 + L^2} \tag{6}$$

The error in determining the lattice parameter for cubic syngony crystals is found by the formula:

$$\Delta a = a \bullet ctg\theta \bullet \Delta\theta \tag{7}$$

Where Δθ – error in determining peak angles on the diffractogram.

The average size of the crystallites was determined using the Debye-Scherrer equation for broadening diffraction maxima, taking into account the instrumental broadening and the software "Powder Cell 2.4". The instrumental broadening was determined at the half-width of the maximum of the standard silicon powder and was 0.14.

The study of the phase composition was carried out on the basis of the fact that each crystalline substance (phase) has a certain crystal lattice characterized by a set of interplanar distances d_{HKL}. The latter are found from the Wolf-Bragg equation, which determines the direction of the diffraction maxima of elastically scattered X-ray radiation on the crystal:

$$2d_{HKL}\sin\theta = n\lambda \tag{8}$$

Where:

d_{HKL} – interplanar distance;
θ – sliding angle (Bragg angle);
λ – wavelength;
n – the order of the diffraction maximum.

The indexing of the radiograph involves the determination of all interference indices (HKL) of each line of the radiograph. In this case, the interference indices are equal to the product of the plane indices (hkl) by the order of reflection n. The indexing of crystal radiographs, depending on the syngony, is based on different ratios. So, for a cubic lattice:

$$a = \frac{\lambda}{2\sin\theta}\sqrt{H_i^2 + K_i^2 + L_i^2} \tag{9}$$

To establish the interference indices of each line, the ratio is used:

$$Q_i = \frac{\sin^2\theta_i}{\sin^2\theta_1} = \frac{H_i^2 + K_i^2 + L_i^2}{H_1^2 + K_1^2 + L_1^2} = \frac{d^2_{H_iK_iL_i}}{d^2_{H_1K_1L_1}} \tag{10}$$

Where Q_i – the line at the smallest angle θ.

Thus, by determining a number of Q_i ratios for all the lines of the X-ray in ascending order, it is possible to determine the type of lattice, interference indices and the period of the unit cell.

One of the methods of qualitative phase analysis is to compare the values of interplane distances and intensities of the studied sample with the reference one. At the same time, the JCPDS-ASTM card file is the most widely used. The calculation took into account both measurement errors of the instruments used and errors due to deviations from the intended ideal solution during the experiment. The error calculation data were compared with the data of statistical processing of the results of the study.

2.4 Scanning Element Analysis

The elemental composition of the sample after electrolytic plasma surface quenching was studied on a scanning electron microscope JSM-6390LV - JEOL (Japan), with the prefix of energy dispersive microanalysis INCA Energy by OXFORD Instruments. When electrons interact with matter, response signals of various shapes arise (reflected and secondary electrons, Auger electrons, X-rays, absorbed current, etc.), which are used to synchronously construct an image on the monitor screen.

Figure 4 shows a diagram of the formation of secondary signals under the influence of an electronic probe. An electron-optical system is not used for image formation, image scaling is carried out by radio engineering means. A scanning electron microscope is a vacuum device, since at normal atmospheric pressures the electron beam is strongly scattered and absorbed, which makes it impossible to focus it.

Therefore, the working vacuum in the microscope chamber should be 10^{-5} Torr or better. The movement of the probe over the surface of the sample should be carried out with very high accuracy. The accuracy of the movement and the size of the probe determine the resolution of the microscope. As a result of the interaction of the electron beam with the sample surface, a response occurs, which is recorded by the corresponding sensors. An electron beam from an electron source is formed by a special condenser system in the form of a well-formed probe and passes through a system of control electrodes or electromagnets that move the beam along the sample surface along a trajectory forming a raster. The signal recorded by the sensors is then used to modulate the brightness of the electron beam in the cathode ray tube of the monitor. The magnitude of this signal will depend on the physical properties of the sample surface and may vary from point to point. As a result, an image of the sample surface is formed on the monitor screen, displaying the topography of the corresponding physical property of the sample under study.

Figure 4. Scheme of formation of secondary signals during the interaction of probe electrons with a sample

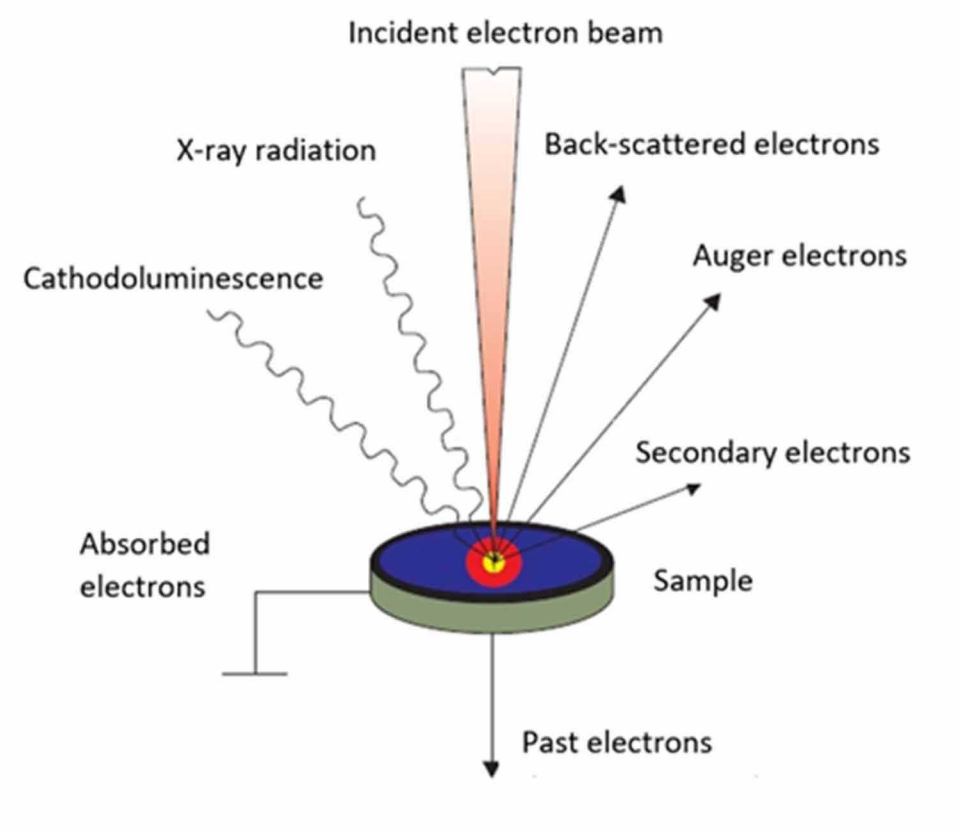

Thus, it is possible to study the topography of inhomogeneities of defects and surface conditions: for example, the topology of the surface (grain boundaries, pores, cracks, inhomogeneities of composition, etc.) – in reflected or secondary electrons. First of all, a scanning electron microscope (SEM) is used to study the structure of the surface. The possibility of studying not only the content of a particular chemical element in the sample, but also the distribution of selected chemical elements over the sample surface makes the scanning electron microscopy method unique.

The energy dispersion method is based on the registration of the so-called characteristic radiation resulting from electron transitions between the internal energy levels of atoms. Depending on the radius of the level, as well as on the binding energy, several types of spectra are distinguished: K, L, M, while only a few X-ray emission lines (K_α, K_β и L- series) are important for materials science (Utevskij, 1973). The use of an energy-dispersive semiconductor detector based on *Si* doped with *Li* in the energy range from 0.7 to 10 keV makes it possible to identify unknown elements. Quantitative elemental analysis consists in finding the concentration of the desired element using the measured intensity of continuous radiation. The mass fraction of an element can be determined by the following formula (Saltykov, 1976):

$$C_i = \frac{I_i \cdot I_{(B)} \cdot C_{(i)} \cdot G_i}{I_B \cdot I_{(i)} \cdot G_{(i)}} \tag{11}$$

Where:

C_i and $C_{(i)}$ – the mass fractions of element i in the analyzed micro-volume of the sample and the standard;
I_i – measured intensity of characteristic X-ray radiation;
I_B – measured intensity of continuous radiation.

The ratio of G-factors takes into account the fact that different intensity of continuous radiation per unit mass in a single volume can be generated in the standard and the sample.

2.5 Transmission Electron Microscopy

Structural studies were carried out using electron diffraction microscopy on thin foils on an EM-125 electron microscope at an accelerating voltage of 125 kV at Tomsk State University of Architecture and Civil Engineering (Tomsk, Russia). The working magnification in the microscope column was 25,000 times. Simplified diagram of a transmission electron microscope showed by Figure 5. The images of the fine structure of steel obtained by viewing in an electron microscope were used, firstly, to classify morphological features of the structure, secondly, to determine the size, volume fractions of the α- and γ-phases, as well as carbide phases and their localization, and, thirdly, to determine the parameters of the fine structure material.

The size and volume fraction of the carbide phases, as well as α- and γ-phases were determined from images confirmed by microdifraction patterns and dark-field images obtained in the reflexes of the corresponding phases. Phase identification was carried out according to the methods described in (Glagolev, 1941). For this purpose, schemes of microdifraction patterns calculated from tabular values of the parameters of crystal lattices were used. For each specific place under study, a large area of foil was viewed on the sample and up to 30-40 micrographs (light-field and dark-field images) and microdifraction patterns were taken.

Preparation of the foil for viewing in an electron microscope was carried out as follows. Plates with a thickness of ~300 microns were cut out on an electric spark machine parallel to the surface of a grade two steel sample that underwent electrolyte-plasma surface hardening (measurements were carried out with a micrometer with an accuracy of 0.01 microns). It should be noted that the electric spark cutting mode was selected in such a way that it did not introduce additional distortions into the structure of the material.

Figure 5. Simplified diagram of a transmission electron microscope

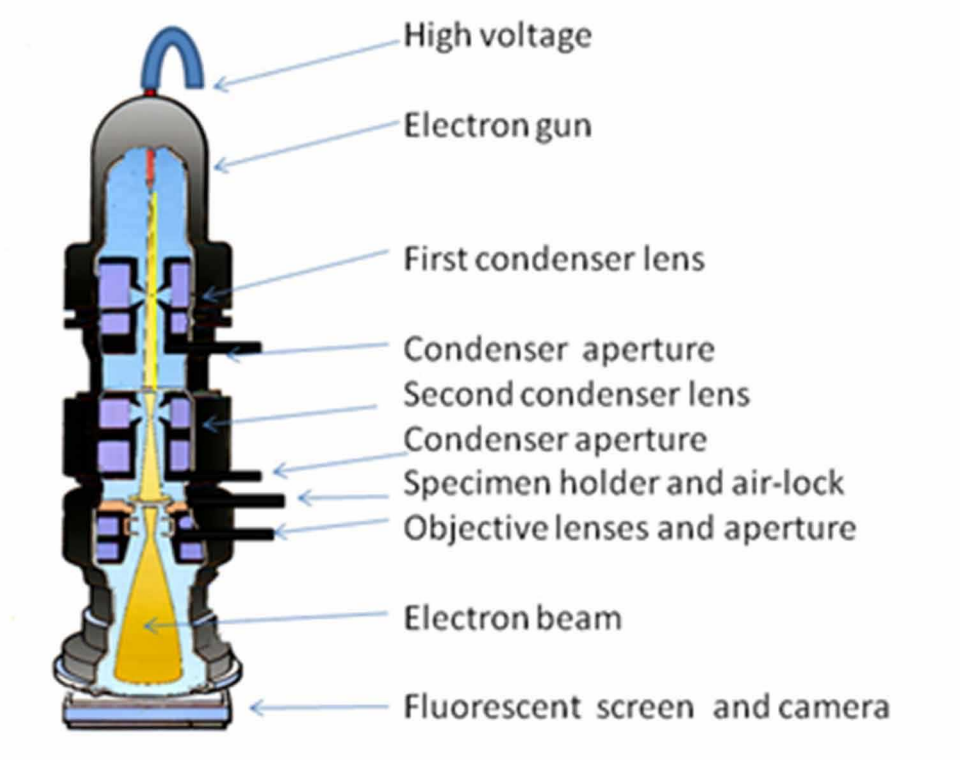

The cut-out plate was cut into two parts. On each part of the plate, one side corresponded to the surface of the processed sample, the opposite side was the side of the cut. A foil corresponding to the near–surface zone of the hardened sample was prepared from one part, and the other part was prepared at a distance of 100 microns from the sample surface.

The foil corresponding to the near-surface zone of the sample was prepared as follows. The surface of the hardened sample was varnished. Then, from the side of the cut, thinning was carried out. The thinning was carried out chemically in a solution of hydrogen peroxide (H_2O_2) with the addition of several drops of hydrofluoric acid (HF). Then, electrolytic polishing was also carried out on the cutting side in a foam of a supersaturated solution of chromium anhydride in orthophosphoric acid at a temperature of 60-80°C. The final stage is the removal of the film from the surface and the final polishing of the sample. Thus, the surface itself was only electrolytically polished for a very short time. Earlier (Malinovskaya, 2006), it was found by the nuclear gamma resonance method that after processing a sample in endothermic atmospheres, films of various iron oxides are always observed in surface zones up to 1 micron deep. Since we were interested in changes in the structure and phase composition of steel occurring in the material at much greater distances from the treated surface, the iron oxides formed on the surface of the sample do not affect the structure of the subsurface layers. Therefore, in order to remove the oxides and not obscure the overall picture, the final electrolytic polishing of the entire sample, i.e. the surface of the sample treated with surface hardening, was carried out for a very short time (~3 seconds). The foil corresponding to the distance from the surface of the sample equal to 100 microns was initially prepared in the same way, i.e. the surface of the hardened sample was also varnished and then thinning

was carried out from the cutting side, first chemically, then electrolytically. But the thinning was carried out only to a thickness equal to ~ 30 microns. After that, the film was removed from the surface of the sample and the final electrolytic polishing was carried out on both sides.

2.6 Microhardness Measurements

Hardness, along with fatigue strength and wear resistance, is one of the most widely used mechanical characteristics of metals and alloys. At the same time, the hardness test differs from other methods for determining the mechanical properties of materials by its high sensitivity and short test time. It is carried out without destroying samples, requires a minimum of costs in their preparation. Measurements of the microhardness of alloy samples were carried out on the PMT-3M device in accordance with GOST 9450-76, with loads on the indenter P = 1H (100g) and the holding time at this load of 10 seconds (Figure 6). In a number of works there is quite complete information about the method of determining the microhardness of materials, about microstructural changes that occur during tests, about the physical nature of microidentification processes. As an indenter for measuring microhardness, a regular four-sided diamond pyramid with an angle at the apex between opposite faces of 136° was used, similar to the determination of hardness by Vickers. Prints were placed on the sample every 100 microns. The number of measurements per sample was at least 30. The microhardness of H_{μ} was determined in accordance with GOST 9450-76 by the formula:

$$H_{¼} = \frac{P}{S} = \frac{1854 \cdot P}{d^2} \left[\text{MPa}\right] \tag{12}$$

Figure 6. General view of PMT-3M

Where d – the diagonal of the print,

$$S = d^2 / 1854 \quad (13)$$

the area of the lateral surface of the resulting pyramidal print.

The tests were carried out on a PMT-3M microhardometer with a LOMO 92063 lens (F=6.3) and with an eyepiece FOM-2-16. The measurement error in accordance with the passport data of the device is 10%. When conducting tests in accordance with the recommendations of GOST 9450-76, the following rules were observed:

- The distance from the center of the print to the edge of the object must be at least twice the size of the print;
- The distance between the centers of neighboring prints should exceed the size of the print by more than 3 times;
- The minimum thickness of the object or layer must exceed the depth of the print by at least 10 times.

Standard computer programs of statistics and correlation analysis were used to process the results of microhardness measurements.

2.7 Tribological Tests

Wear resistance tests were carried out at the installation of the Scientific Research Center "Surface Engineering and Tribology" at the Sarsen Amanzholov East Kazakhstan University for testing materials for abrasive wear (Skakov & Rakhadilov, 2012). The wear resistance of the tested material was evaluated by comparing its wear with the wear of the reference sample (steel 45) according to GOST-23.208-79. The relative wear resistance of the tested steel was calculated by the formula:

$$K_{tm} = \frac{g_{rs} \cdot \rho_{tm \cdot N_{tm}}}{g_{tm} \cdot \rho_{rs} \cdot N_{rs}} \quad (14)$$

Where g_{rs}, g_{tm} – the values of mass loss during testing of the reference sample and samples of the test material, g; ρ_{rs}, ρ_{tm} – density of the reference and test material, g/cm^2; N_{rs}, N_{tm} – the number of revolutions of the roller when testing the reference and test materials.

Tribological dry friction tests were carried out at the center for collective use of TSU, Tomsk, Russia, where a high temperature tribometer (TNT, CSMInstruments, Switzerland) was used, as well as at the TRIBOMETER TRB^3 (Anton Paar) installation at the Scientific Research Center "Surface Engineering and Tribology" at the Sarsen Amanzholov East Kazakhstan University.The tests using the tribometer were based on the measurement by the LVDT sensor of the friction force that occurs when a spherical fixed counterbody pressed with a given force against the sample slides. Tribological measurements were carried out in air (30±5 ° C) in dry friction mode according to the "ball-disc" scheme (Figure 7) in accordance with international standards ASTMG-99 using a counterbody (ball with a diameter of 6 mm) made of Al_2O_3. The load on the counterbody was 5 N. The linear velocity was 2 cm/s. The friction path

Figure 7. Scheme of testing samples for wear resistance using the "ball-disc" method

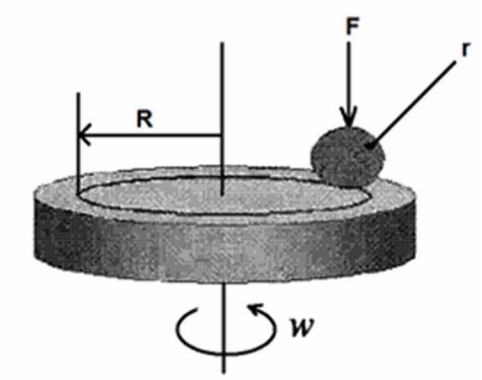

is 31.4 m. In the course of the study, the analysis of wear products, as well as the contact area on the counterbody, was carried out by examining the structures of wear grooves on the surface of the coatings under study, as well as changes in wear spots on the ball. Measurements of the vertical section of the wear grooves were carried out on a profilometer in four diametrically and orthogonally opposite areas, after which the average value of the groove depth and cross-sectional area was calculated.

The surface profile was measured using a profilometer device by measuring the vertical deflection of a diamond tip (probe) moving at a constant speed under conditions of mechanical contact with the sample. The device has a multifunctional RS-232 port, with which it is possible to transfer data to a printer for printing or to a computer for subsequent analysis using additional Talyprofile software. The software allows you to calculate parameters, set calculation modes in full compliance with international standards.

2.8 The Method of Electrolytic-Plasma Surface Hardening

Electrolyte-plasma surface quenching in cathode mode was carried out at the electrolyte-plasma treatment plant at the Scientific Research Center "Surface Engineering and Tribology" at the Sarsen Amanzholov East Kazakhstan University (Tabieva, Rahadilov, Uazyrhanova, et al, 2020).

The installation for conducting electrolyte-plasma surface hardening structurally consists of a power source, a material processing chamber and a personal computer. Table 2 shows the main technical characteristics of the installation.

A schematic representation of the installation (Figure 8) for electrolyte-plasma surface quenching (Tabieva, Rahadilov, Uazyrhanova, et al, 2020), and the processing process (Figure 8b) is shown in Figure 8. A rectifier was used as a power source for the EPSH installation, which gives a maximum output of 360 V /60 A in the form of direct current. Considering that the output of power supplies with the necessary electrical parameters is limited, the power supply of the installation for conducting electrolyte-plasma treatment was produced by a powerful rectifier manufactured by the authors of the works (Rahadilov, 2014). The manufactured DC power supply consists of a welded frame reinforced on the base of a transformer for lowering with a power of 40 kW. The power supply of this source is carried out from a three-phase AC network with a frequency of 50 Hz and a voltage with a maximum value of 380 V. The power supply is controlled by the buttons marked "Start" and "Stop" which are located on the front panel of the housing of this source. A fuse is installed to protect the circuits from short circuits.

Figure 8. Schematic representation (b) of the installation and processing of the sample mounted on the holder with electrolyte plasma in an aqueous electrolyte solution (a)
1– samples; 2 – cone–shaped stainless-steel cell; 3– pallet; 4–pump; 5- heat exchanger; 6– bath with electrolyte.

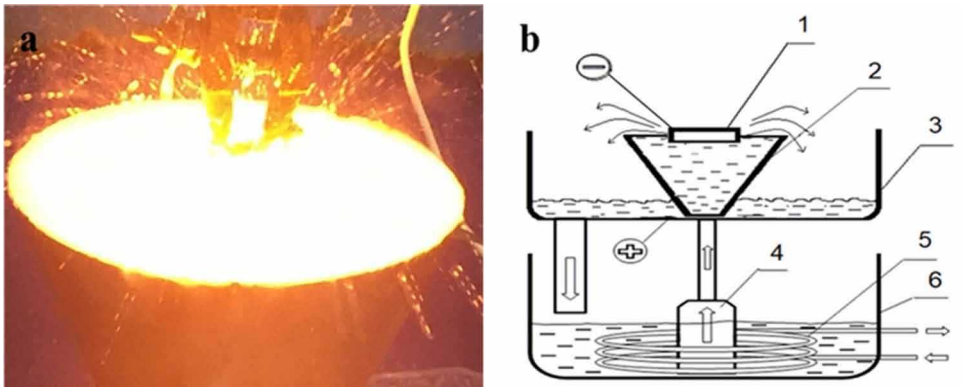

Table 2. Technical characteristics of the installation

Name of the Parameter	Meaning
Supply network voltage, V	380
Supply network current frequency, Hz	50
Maximum power consumption not more than, kW	40
Output voltage, V	0 to 350
Output current, A	0 to 60
Overall dimensions of the power supply, not more than, mm	700×440×600
Overall dimensions of the installation chamber, not more than, mm	660×660×1520
Weight of the power supply, not more than, kg	150
Weight of the installation chamber without solution, not more than, kg	40

Adjustable voltage for the electrolyte-plasma treatment process within the values U = from 0 to 360 Volts, the current value is up to I = 100 Amperes (Rahadilov, 2014).

For EPSH, we selected the following electrolytes containing carbamide and sodium carbonate with different concentrations indicated in Table 3. becouse for surface hardening of steels, aqueous solutions of sodium carbonate are most widely used. As is known (Rahadilov, 2014), for the cathode process, the most optimal component providing a stable discharge is sodium carbonate. In this regard, an electrolyte based on sodium carbonate was chosen for surface hardening. In order to prevent the decarburization process, carbamide was added to the electrolyte. The choice of urea is due to the fact that this substance is a source of carbon, and is also characterized by cheapness and environmental safety. It is also important to note that urea is highly soluble in water: at 20 ° C, the solubility of urea is 51.83% (by weight). In addition, sodium carbonate interacts well with urea. In this regard, sodium carbonate was chosen as the component providing the optimal value of the electrolyte's electrical conductivity, and carbamide was chosen to prevent decarburization of the surface.

Table 3. Working composition of water-based electrolytes

Electrolyte No.	Na_2CO_3, %	$(NH_2)_2CO$, %	H_2O, %
1	10	10	80
2	20	10	70
3	15	15	70
4	10	20	70
5	20	20	60

In general, the hardening process is carried out as follows: before starting work, the working bath is filled with electrolyte. Then the electrolyte enters the electrolytic cell using a pump installed at the bottom of the working bath. In this case, the electrolyte exits through the opening of the cone-shaped partition in the form of a jet and fills the electrolytic cell. Then the electrolyte is drained through the edge of the electrolytic cell into the pan, and then back into the working bath. Thus, the electrolyte is in circulation mode. For conducting electrolytic-plasma surface hardening, the test sample made of grade two steel is installed and clamped (Figure 8b) using a clamping mechanism (1) over a cone-shaped electrolytic cell (2) made of stainless steel, for conducting electrolytic-plasma surface hardening (Tabiyeva et al., 2019). A pump (4) is also used, which has a liquid electrolyte supply regulator, thereby ensuring that the electrolyte temperature is cooled to the required value (maintained at 25 ± 1°C). And the used aqueous electrolyte solution from the tray (3) is fed into the working bath (6) thereby ensuring circulation of the working electrolyte. Measurements of temperature values and temperature control of the active electrode and the working electrolyte are carried out by a digital multimeter "UNI-T" and UT-70B with built-in thermocouples (Rahadilov, 2014).

The very process of electrolytic-plasma surface quenching is controlled by a personal computer, which smoothly and with sufficiently high accuracy allows you to adjust the main energy parameters of the working plasma jet, as well as the dynamics of movement of the studied part (sample) undergoing plasma quenching. The depth of immersion of the sample or the working surface of the part in the working electrolyte can be adjusted by means of a clamp (1) moving up and down.

Conclusions on the Section

In the total volume of steel production, carbon steels make up the majority, which are widely used due to the relatively simple method of production and low cost. Parts made of this class of materials determine the performance of the product as a whole. In accordance with the tasks set, grade two bandage steel used in the field of metallurgy and mechanical engineering was selected as the research material for the manufacture of bandages for freight, passenger and shunting locomotives, subway cars and wheel bandages for pairs of tram cars that are subject to wear during operation and require hardening of their wear surface.

The considered types of surface hardening, according to their final results of the structural-phase state, hardness and wear resistance of the hardened layer, are equivalent, but differ in labor intensity, equipment cost and other technical indicators that determine the cost of processing. One of the promising methods of quenching with highly concentrated heating sources is electrolyte-plasma surface quenching, characterized by relatively lower energy consumption, simplicity of technological equipment and large

size of the hardened zone. Phase and structural transformations in carbon steels during surface hardening play an important role, since the formation of defects and wear during operation largely depend on the structural components of the surface layer. The properties of various structures of the surface layer depend on the mechanism of formation, shape, size, density of dislocations of the hardening phase, which are formed during electrolyte-plasma surface quenching. To elucidate the physical mechanisms of the formation of structural-phase states and fine structure during electrolyte-plasma surface quenching, which provide an increase in hardness and wear resistance, their analysis by metallographic research using optical, scanning and transmission electron microscopy of high resolution, as well as X-ray diffraction analysis is necessary.

3. CHANGE IN THE MECHANICAL PROPERTIES OF THE SURFACE OF GRADE TWO STEEL AS A RESULT OF ELECTROLYTE-PLASMA SURFACE HARDENING

In this section are presented, the results of studying the effect of a hardened surface layer during plasma quenching in the cathode mode on the mechanical and tribological characteristics of grade two wheel steel.

3.1 Change in the Surface Hardness of Steel grade two During Electrolytic-Plasma Surface Quenching

Being one of the varieties of plasma quenching – electrolyte-plasma surface quenching (EPSQ) has recently been developing and intensively studied. This method is characterized by lower energy consumption, simplicity of technological equipment and large size of the hardened zone. One of the most important properties of the working, surface layer of parts, which significantly affects the quality of wear resistance of this part, is hardness. In this paper, studies have been carried out to study changes in the microhardness values of the surface layer of grade two wheel steel after EPSQ in an electrolyte from an aqueous solution containing 20% sodium carbonate and 10% urea (Rakhadilov, et al., 2019).

Figure 9. Microstructure of grade two steel before (a) and after EPSQ (b)

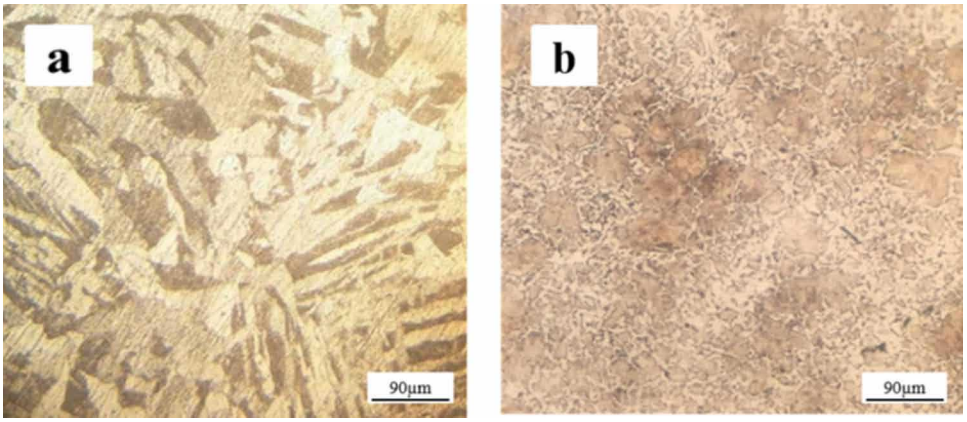

Figure 9 shows the surface structure of the initial and processed samples. Metallographic analysis showed that in the initial state, grade two steel has a ferrite-pearlite structure of carbon steel. The amount of ferrite is 35% (Rakhadilov, et al.,). After EPSQ with a heating duration of 2 s, the microstructure changes, a quenching effect is observed, and martensite is formed on the surface. The formation of a cementite mesh in the structure of grade two steel as a result of the EPSQ, which is located around the ferrite, significantly increases the microhardness of grade two steel. According to (Tabiyeva et al., 2020) the results obtained (Figure 10), the average values of microhardness in the surface hardening zone is ~ 420 HV, in the zone of thermal influence is ~ 260 HV and, accordingly, in the matrix of grade two steel, the microhardness value remained unchanged ~ 140 HV.

Figure 10. Microhardness of the cross-section of samples steel of grade two after EPSQ

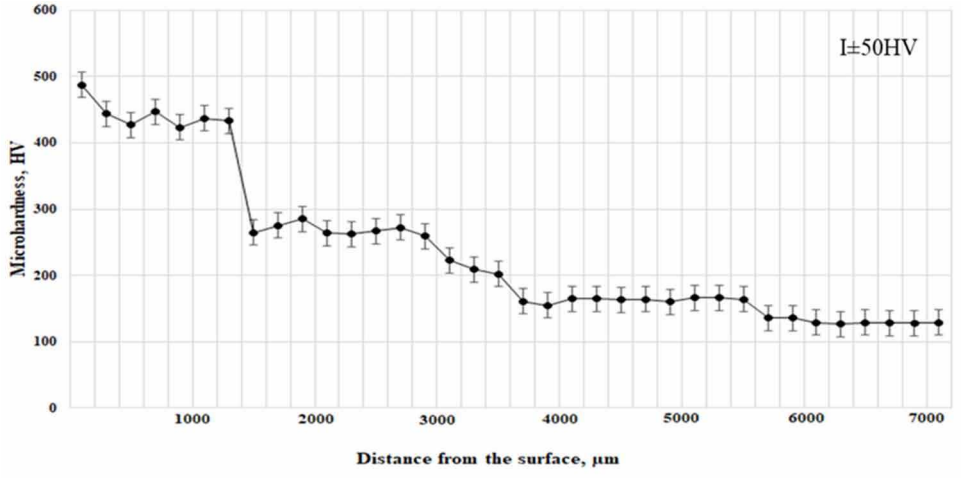

Figure 11. X-ray phase analysis of steel grade two

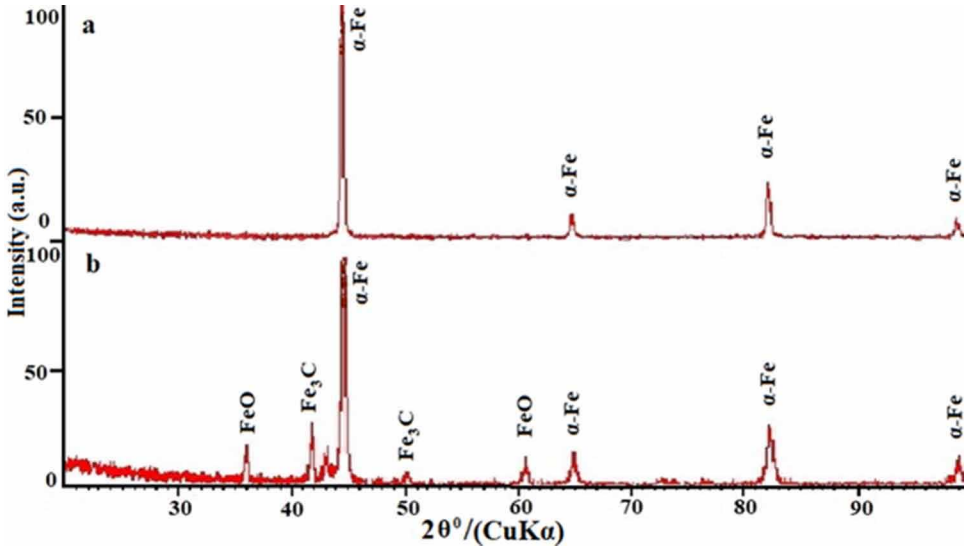

Figure 12. Cross-section microstructure images of grade two steel after EPSQ a) hardened layer; b) transition layer; c) uncured layer; d) general appearance.

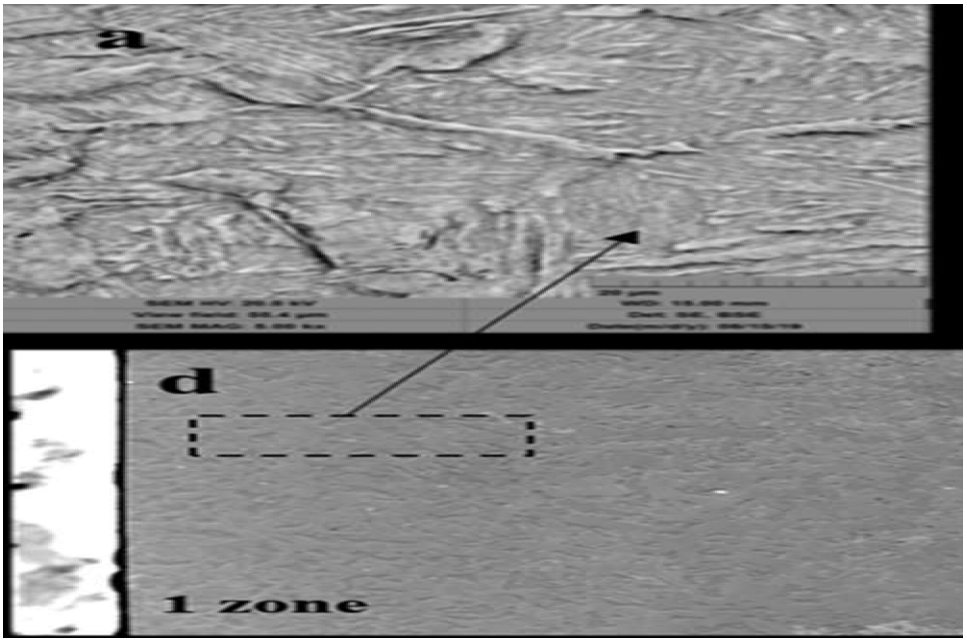

Structural changes were also detected during the study of the microstructure of the near-surface layers of grade two steel samples subjected to electrolyte-plasma surface quenching in electrolyte plasma.

Figure 11 shows X-ray diffractograms of grade two steel before and after the EPSQ. The obtained diffractograms show that after EPSQ, martensite, cementite, and iron oxide are formed on the surface of the steel. I would like to note (Bayatanova, 2014) that X-ray diffraction analysis determines the presence of any phase with its content in an amount of at least 2%. To identify the phases formed in the process of EPSQ in smaller proportions, the method of transmission electron microscopy is used.

Figure 12 (a-b) shows a snapshot of the microstructure of the cross-section of steel after treatment in electrolyte. As can be seen from Figure 12, electrolyte-plasma surface hardening led to a change in the microstructure of the cross-section of the sample, where the zoning of structures typical of electrolyte-plasma treatment is visible (Uazyrkhanova et al., 2020). To be more precise, the cross-section structure consists of 3 zones:

Zone 1 – surface hardening zone with a thickness of 1000-1500 μm,
Zone 2 is a zone of thermal influence,
Zone 3 is a matrix (initial structure).

Also, only using the method of electron transmission microscopy it is possible to obtain experimental data on the fine structure of the material, which will allow us to study the changes that have occurred both on a qualitative and quantitative level, which was done with samples of grade two steel, the results of which are described in detail and given in section 4 of this chapter. The microstructure of the surface of a hardened steel sample of grade two is a fine-grained ferritic structure. The formation of a modi-

fied layer of fine-grained ferrite with cementite particles in the surface layers will positively affect the operational properties of the parts.

3.2 The Effect of Electrolyte-Plasma Surface Quenching on the Tribological Properties of Wheel Steel

The mechanism of wear of parts during operation is complex and includes abrasive, adhesive and diffusion wear. Wear resistance tests were carried out according to the "ball – disk" and "flat surface – rotating disk" schemes.

Tribological properties of samples before and after EPSQ were investigated. Experimental curves of the dependence of the coefficient of friction on the friction time of the initial and processed samples are shown in Figure 13. The test was carried out according to the "ball-disc" scheme, the run length was 31 m, the speed was 2 cm/ s, the load was 5 N. It can be seen from Figure 13 that the coefficient of friction of steel samples of grade two before and after the EPSQ with a heating duration of 2 seconds increases from 0.12 to 0.42, then decreases to 0.4-0.338 and remains at this level until the end of friction. This is due to the roughness of the surface, as well as the unevenness of the surface layer in depth, i.e. the fragmented ferritic structure with the cementite mesh formed on the surface smoothly transitions into a ferrite-pearlite structure. The experimental curves of the dependence of the coefficient of friction on the length of the run are shown in Figure 14. The test results showed that the average coefficients of friction at a normal force of 5 N and the speed of mutual displacement of 2 cm/s are in the range from 0.27 to 0.40, which possibly indicates the destruction of the surface layer of the samples under study. All processed indicators have a good degree of improvement in tribological properties.

The tribological characteristics of the samples before and after EPSQ were characterized by the intensity of wear, the average values of which were $4.83 \cdot 10^{-4}$ mm^3/N·m before quenching and $2.04 \cdot 10^{-4}$ mm^3/N·m after quenching. After EPSQ samples, there is an increase in wear resistance under dry friction conditions. With the help of a profilometer, images of the contact zone of the initial and processed EPSQ steel samples of grade two were taken (Figure 15).

Figure 13. Friction coefficient of steel grade two before (a) and after (b) EPSQ

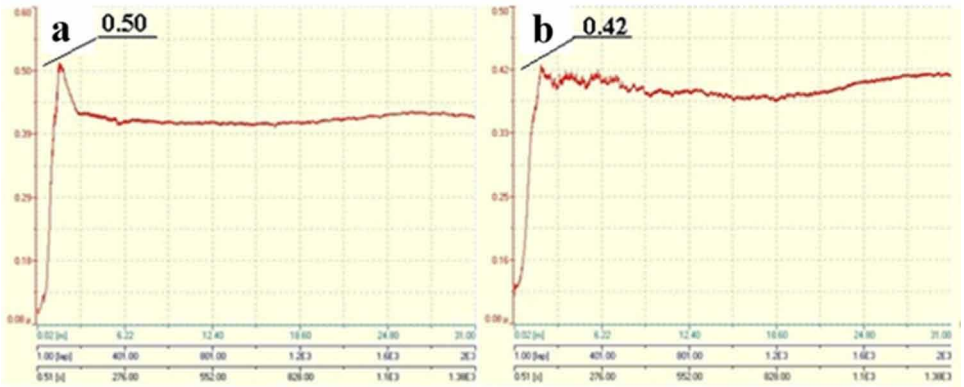

Figure 14. Friction coefficient of steel grade two before and after EPSQ: (b) initial; (c) 2 s; (d) 3 s; (e) 4 s

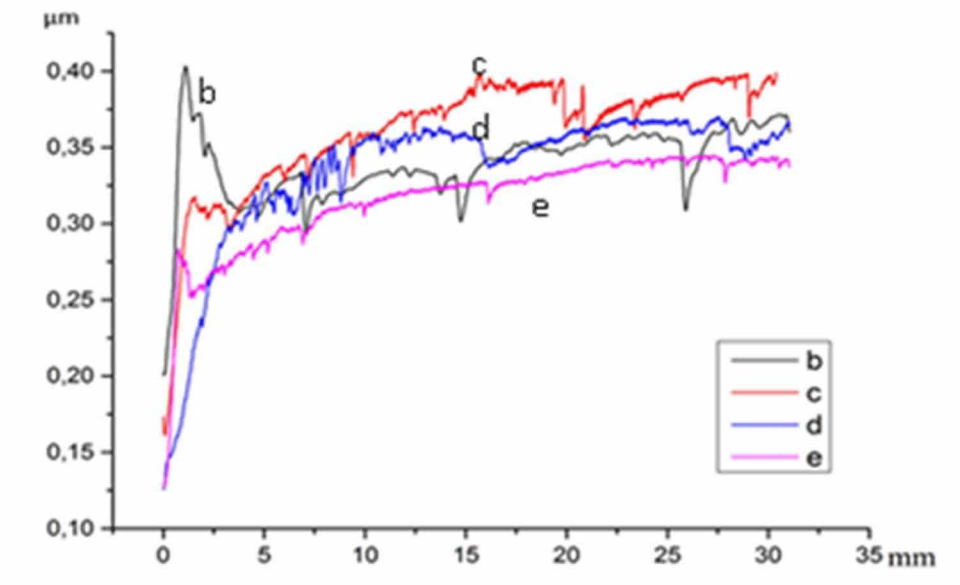

Figure 15. Profiles of the tracks of the initial (a) and hardened EPSQ (b) samples of steel grade two

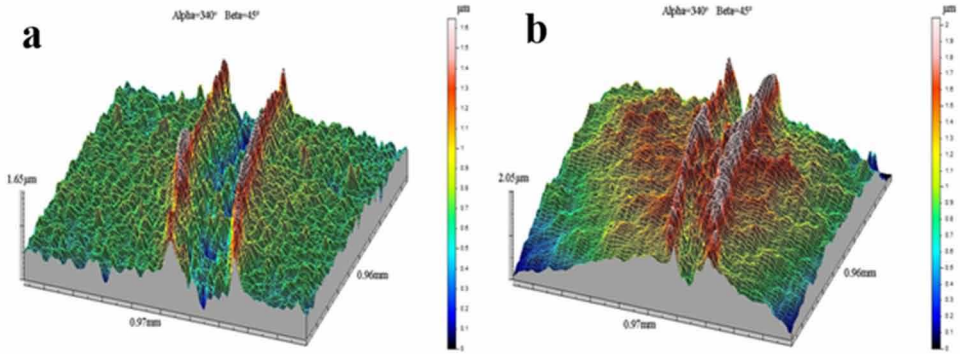

The results of the tests of the samples for abrasive wear were evaluated by the loss of mass of the samples after the test. The mass loss values of grade two steel samples before and after EPSQ were 0.0796 mg±0.01mg and 0.0231 mg±0.01mg, respectively. A significant increase in wear resistance is observed on all samples subjected to EPSQ.

To clarify the structural factors affecting the wear resistance, hardness and other characteristics of steels, the structural and phase states of the hardened surface layers of grade two steel were studied. Based on the X-ray phase results obtained, it can be said that during electrolytic plasma surface quenching, the surface layer of steel is saturated with carbon and martensite, cementite and oxides are formed on the surface layer iron. The thickness of the modified layer is 0.6-1 mm.

Conclusions on the Section

Based on the analysis of the results of the experimental work, a method for processing wheel steel by electrolytic-plasma surface quenching in an electrolyte from an aqueous solution containing 10% carbamide $(NH_2)_2CO$ and 20% sodium carbonate Na_2CO_3 has been developed.

The formation of hardening phases present on X-ray diffraction images, as a result of electrolytic-plasma surface hardening of grade two steel, led to an increase in the microhardness of the sample surface, the average values of which in the surface hardening zone are ~ 420 HV, while in the steel matrix the microhardness value remained unchanged ~ 140 HV.

It is established that the developed method of electrolyte-plasma quenching makes it possible to obtain a modified layer with a thickness of 1000-1500 microns with increased hardness, corrosion resistance and wear resistance by 2.5 – 3.8 times due to the formation of a fragmented structure of packet-plate martensite and carbide particles of the second phases.

4. STRUCTURAL AND PHASE STATE OF GRADE TWO WHEEL STEEL BEFORE AND AFTER ELECTROLYTIC PLASMA SURFACE QUENCHING

This section of the paper describes the phase composition and morphology of grade two steel in its initial state and after electrolytic-plasma surface quenching. These descriptions are accompanied by images obtained by transmission electron microscopy. The light-field images and micro-diffraction patterns obtained from these sites, as well as their dark-field patterns, are given.

Figure 16. Crystal lattices ●– iron atom, ○– carbon atom, ○ – octahedral (a) and α – tetrahedral (b) internodes, some of which may be occupied by carbon atoms, (c) – cementite (Fe3C iron carbide)
Source: Uazyrkhanova et al. (2020)

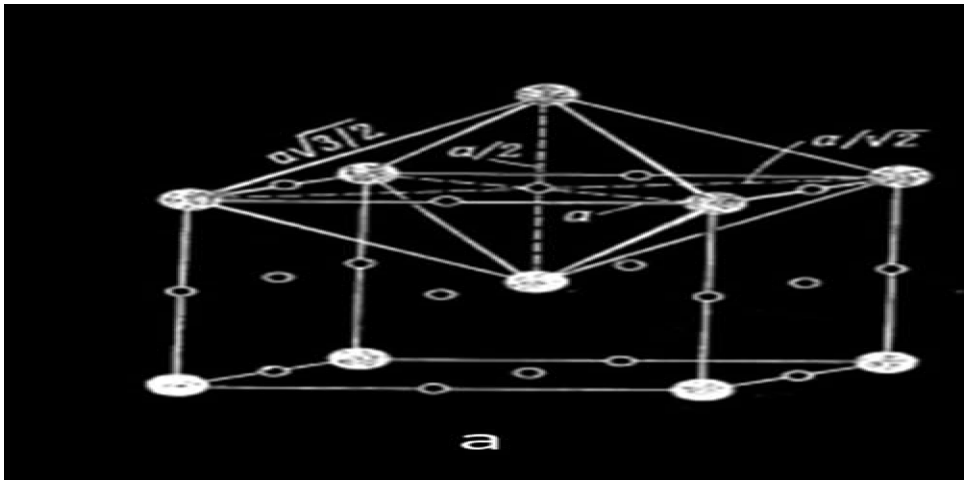

4.1 Initial Structure and Phase Composition of Grade Two Steel

The study was carried out both on a qualitative and quantitative level using the method of transmission electron diffraction microscopy on thin foils. All the data obtained were processed statistically. Phase identification was carried out according to the methods discussed in (Ivanov, & Kozlov, 1991; Ivanov & Kozlov, 2002; Kozlov, et al., 2004).

For this purpose, schemes of microdifraction patterns calculated from tabular values of the parameters of crystal lattices were used. The conducted studies have shown that in the initial state, the steel matrix is a α-phase – a solid solution of carbon and alloying elements in α-Fe. The α-phase has a body-centered cubic (BCC) lattice (Figure 16) and can be solid solutions based on iron atoms of introduction (C, N, B, S, P, etc.) and substitution (Si, Mn, Ni, Cr, Mo, V, W, etc.) simultaneously.

The morphological components of the α-phase are lamellar perlite (LP) and ferrite. Lamellar perlite, almost perfect, i.e. it is a conglomerate of alternating parallel plates of ferrite and cementite (Abuali Galedari, & Mousavi Khoei, 2013). Ferrite (α-phase) in perlite has a body-centered cubic (BCC) crystal lattice.

Cementite, which is a chemical compound of carbon with iron (Fe_3C iron carbide), has an orthorhombic crystal lattice. The carbon content in cementite is 6.67 wt.%. Cementite in perlite can be alloyed, i.e. iron atoms can be replaced by nonmetal atoms: nitrogen, oxygen, boron, and iron atoms by metals: manganese (in unlimited quantities), chromium (up to 20%), molybdenum (up to 2%), vanadium (tenths of %), etc. Pure carbonaceous cementite is a metastable phase and the entire $Fe–Fe_3C$ diagram is also metastable. This fact has a noticeable effect on the properties of steels of this class. The mutual parallelism of the plates means that:

- different plates of the same phase within the colony have the same orientation;
- the mutual orientation of the two phases (their orientation ratio) ensures the best coupling of the two crystal lattices along the habitus surface of the plates.

It has been established (Suhomlin,) that the orientation relation of Bagaryatsky is observed between ferrite and cementite in almost every pearlite colony. It should be noted that the effect of steel alloying on the crystallographic characteristics in perlite has not been established (Popova, et al., 2020). The electron microscopic image of lamellar perlite (LP) obtained during the study is shown in Figure 17.

Figure 17 shows that in the initial state, grade two steel is a ferrite-perlite mixture and that cementite particles have a lamellar shape, are located almost parallel to each other, and there are clear reflexes on the microdiffraction pattern (Figure 17b), which are identified (Figure 17c) like cementite reflexes. The black arrow (Figure 17a) indicates the coinciding directions $[011]_{\alpha} \,||\, [21\bar{1}]$ at the same time $\left(13\bar{3}\right)_{\alpha} \,||\, \left(1\bar{2}0\right)_{C}$ – Bagaryatsky ratio. The volume fraction of lamellar perlite is 35% in the volume of the material. Note that to determine the volume fraction, a planimetric method was used, which boils down to measuring the total cross-sectional area of this structural component on a certain area of the foil. It can be seen from the presented figures that the dislocation structure in ferrite plates represents dense dislocation grids. The average scalar dislocation density ρ was calculated by the rectangular grid method (Kozlov, et al., 2014). The calculations performed showed that the average scalar dislocation density in ferrite plates is equal to 2.1×10^{10} cm^{-2}. Dislocations are not allowed in cementite plates. As

Figure 17. Electron microscopic image of the fine structure of the initial state of the grade two wheel steel (FF – fragmented ferrite; LP – lamellar perlite) a – is a light–field image; b – is a micro–diffraction pattern obtained from the area marked on (a) with a circle; c – is its indexed scheme containing the reflexes of the α-phase and cementite.

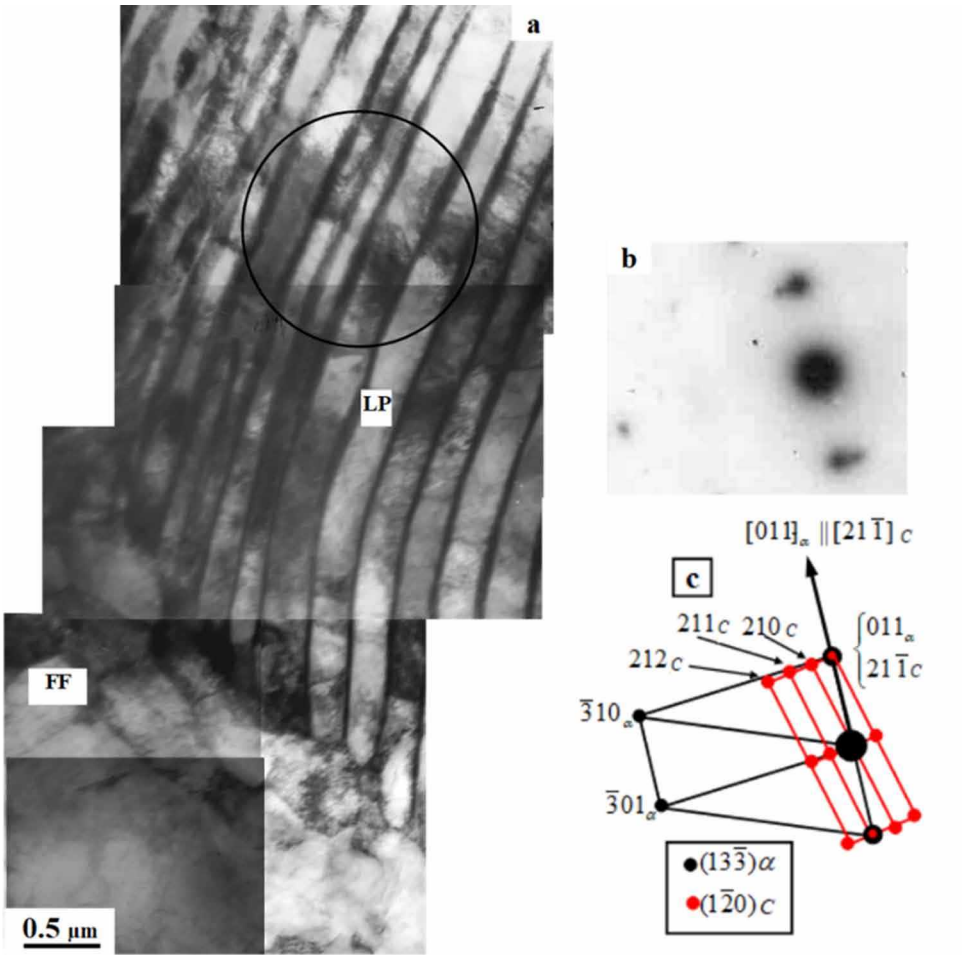

shown by the studies carried out on a transmission electron microscope, ferrite is present in the initial state of grade two wheel steel in the form of unfragmented ferrite (UF) and fragmented ferrite (FF).

Unfragmented ferrite – in the studied wheel steel, these are individual grains that are shown in Figures 18 and 20. The dislocation structure of unfragmented ferrite, as in perlite, is represented by dislocation grids, the average scalar dislocation density is 2.57×10^{10} cm^{-2}.

According to the conducted studies of the initial state of the grade two wheel steel, no carbide phase was detected either inside the grains or at their boundaries on a transmission electron microscope. This is evidenced by microdifraction patterns obtained from grains of unfragmented ferrite. One such example is shown in Figure 18 and Figure 20.

Figure 18. An image of the fine structure of the initial state of grade two steel obtained using a transmission electron microscope (UF – unfragmented ferrite)

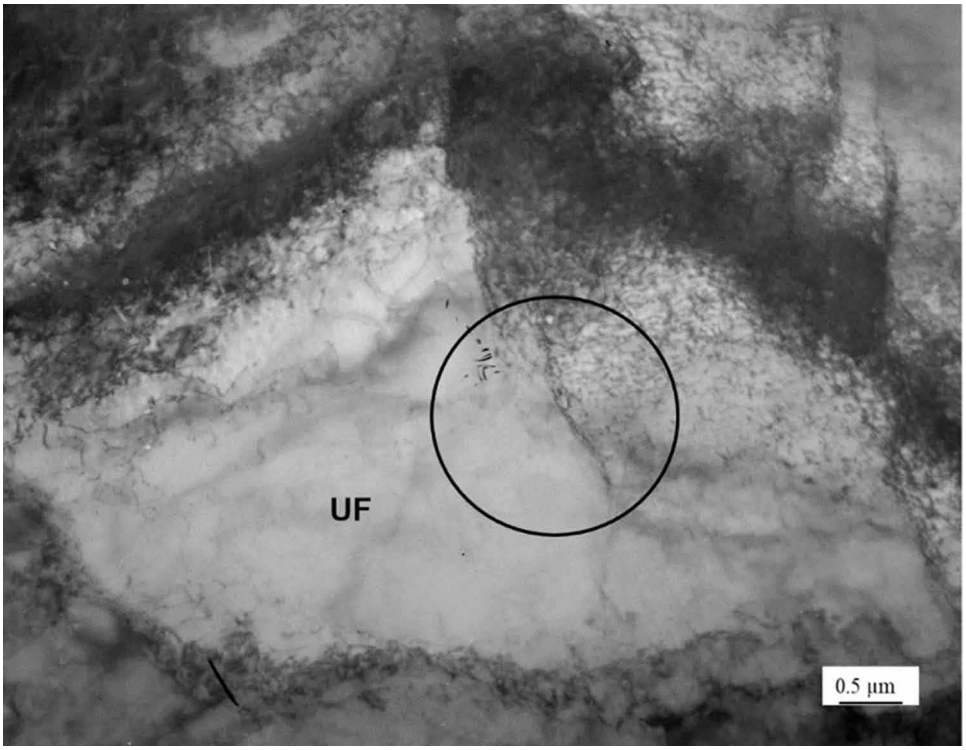

Figure 19. Microdifraction pattern (a) obtained from a grain section of unfragmented ferrite and its indexed scheme (b)

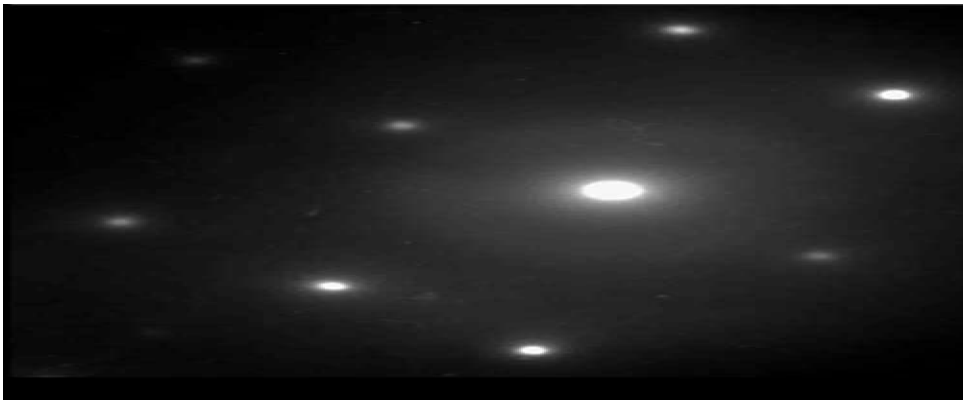

Figure 19 shows a microdifraction pattern (a) obtained from a grain section of unfragmented ferrite highlighted with a black circle in Figure 19 and its indicated scheme (b), where it is seen that reflexes belonging only to the α-phase are present in the initial state. According to the calculations performed, the volume fraction of unfragmented ferrite in the material is ~ 10%.

Figure 20. An image of the fine structure of the initial state of grade two steel obtained using a transmission electron microscope (UF – unfragmented ferrite; FF – fragmented ferrite)

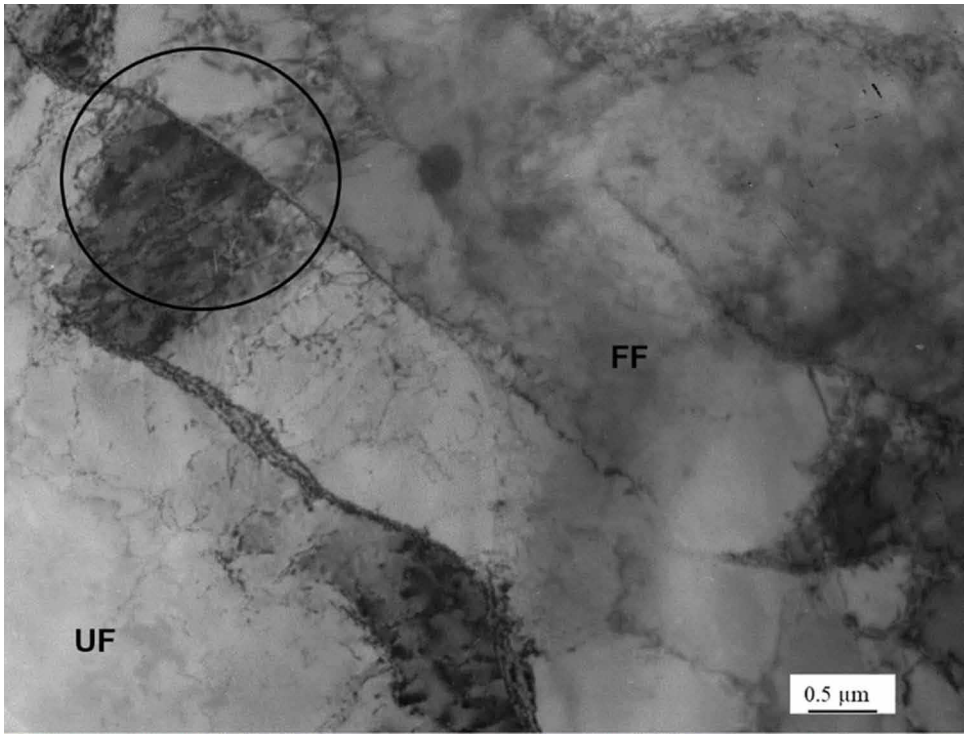

Figure 21. Microdifraction pattern (a) obtained from a grain section of fragmented ferrite and its indexed scheme (b)

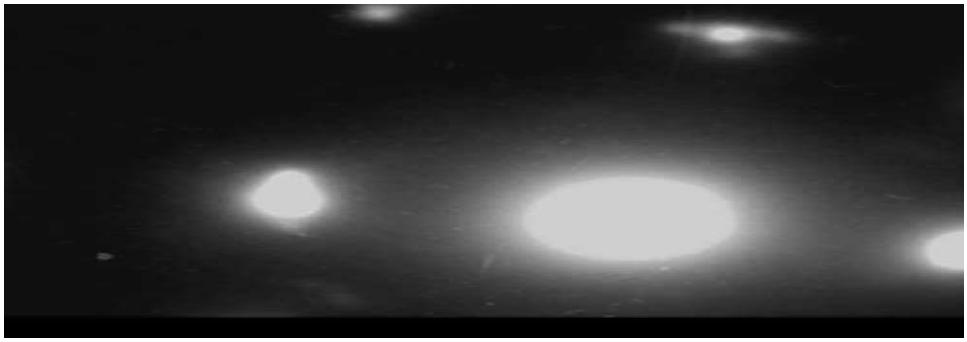

Fragmented ferrite is a substructure that consists of dislocation sub–boundaries (fragment walls) and an internal space containing or not containing dislocations. According to the calculations performed, the volume fraction of fragmented ferrite was 55% (Popova, et al., 2020). The dislocation structure inside the fragments is also mesh. The average scalar density in fragmented ferrite is almost the same as in unfragmented and amounted to 2.89×10^{10} cm^{-2}.

Figure 22. Electron microscopic image of the fine structure of the initial state of grade two steel (P – perlite; UF – unfragmented ferrite; FF – fragmented ferrite) a – ferrite-pearlite mixture; b – enlarged image of the area marked with a black circle on (a).

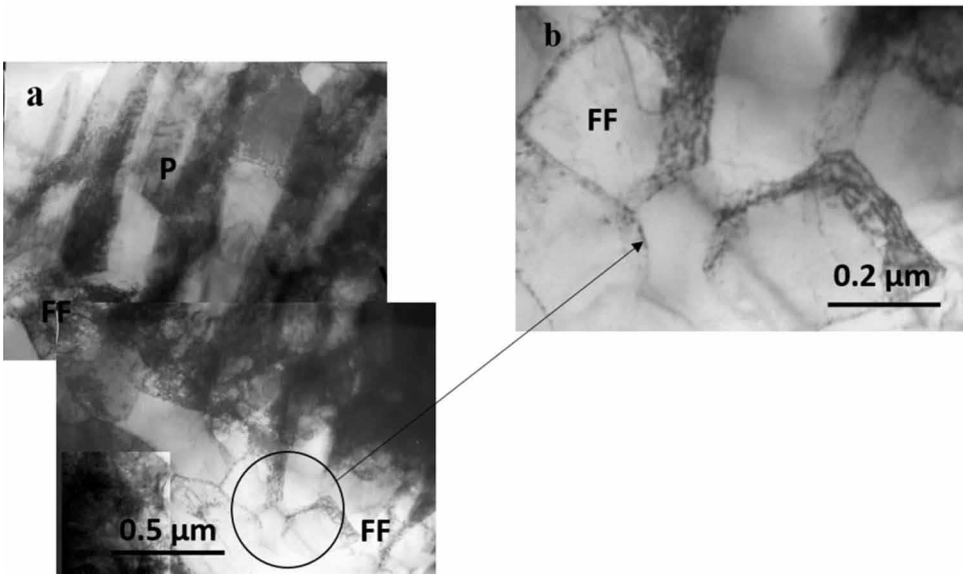

The boundaries of the fragments are free of carbides, and the carbide phase is also not detected inside the fragments. The proof of this is the microdifraction pattern shown in Figure 21a, obtained from a section of fragmented ferrite highlighted by a black circle in Figure 20 and its indexed scheme shown in Figure 21b – shows that there are reflexes belonging only to the α-phase.

According to the calculations carried out, the average size of fragments of fragmented ferrite is ~1 microns (Figure 22) (Tabieva, Popova, Nikonenko, et al, 2020). As studies have shown, at the joints of "perlite – ferrite" grains, there are often either groups of small (~0.3 microns) fragments, or chains of very small (0.08 microns) fragments, which is clearly visible in Figures 18-22, the area marked with a black circle, an enlarged image of which is shown in Figure 22b. This indicates that the fragmentation of ferrite began from the grain boundaries of "perlite – ferrite" (Rakhadilov, et al., 2020).

4.2 Quantitative Parameters of the Fine Structure of Grade Two Steel Before Electrolytic-Plasma Surface Hardening

The dislocation structure in both perlite and ferrite is polarized. This is indicated by the presence of flexural extinction contours in the entire material. We emphasize that such contours are not the result of deformation of the sample during the manufacture of thin foil from it, because the technique used in the preparation of foils almost completely eliminates the introduction of artifacts. The presence of extinction contours is the result of bending of the crystal lattice, or bending of the crystal α-matrix. At the same time, only a small part of the crystal is in the exact reflecting position (contour). The smaller the contour width, the more curved the crystal is. By measuring and calculating the average thickness (the value of the transverse dimension) of the extinction contour in any part of the material, it is possible to determine the χ-amplitude of the curvature-torsion of the crystal lattice. For each morphological

Table 4. Average quantitative parameters of the morphological components of the fine structure and in general for the material in the initial state of grade two steel

Morphological Component	Average Quantitative Parameters of Fine Structure					
	P_V	ρ, cm^{-2}	$\rho_{\pm}$, cm^{-2}	χ, cm^{-1}	σ_{Sh}, MPa	σ_{∂}, MPa
Perlite	35%	2.10×10^{10}	1.44×10^{10}	360	285	240
Unfragmented ferrite	10%	2.57×10^{10}	1.46×10^{10}	365	320	240
Fragmented ferrite	55%	2.89×10^{10}	2.76×10^{10}	690	340	330
In general, according to the material	100%	2.54×10^{10}	2.10×10^{10}	525	315	285

component: in perlite, unfragmented and fragmented ferrite, as well as for the whole material in the initial state of grade two steel, the following quantitative parameters of the fine structure were calculated according to the scalar dislocation density - ρ and the size of the bending extinction contours: χ, $\rho_{\pm}$, σ_{∂} and σ_{Sh}, the average values of which are shown in Table 4.

Analyzing the data indicated in Table 4, it can be argued that:

- the highest quantitative parameters were in fragmented ferrite, the lowest – in perlite.
- the conditions are met in all the material: $\rho > \rho_{\pm}$ and $\sigma_{Sh} > \sigma_{\partial}$.

This means that the bending-torsion (distortion) of the crystal lattice of the grade two wheel steel in its initial state is purely plastic in nature, which does not lead to the formation of microcracks in the material.

4.3 Structure and Phase Composition of the Near-Surface Zone of Wheel Steel After Electrolytic-Plasma Surface Quenching

The conducted studies have shown that the surface hardening of grade two steel has led to significant qualitative and quantitative changes, namely, to a change in the phase composition and the list of phases present, as well as their morphology. Thus, both the phase composition and the fine structure of the steel after surface hardening differ significantly from the initial state.

The surface hardening carried out led to the formation of packet-plate martensite. Electron microscopic images of the resulting structure are shown in Figures 23-27. It is known that martensite is a supersaturated solid solution of carbon in α-iron with the same concentration of dissolved carbon as the original austenite. It is also known that in high-carbon, low-alloy steels, batch (or rack-and-pinion), lamellar low-temperature and lamellar high-temperature martensite is formed. It was to this structure that the surface hardening of grade two steel led. Batch (or rack-and-pinion) martensite is a structural formation consisting of a set of elongated crystals (slats) almost parallel to each other, forming a package. A separate package has a certain shape and size. The shape of the cross-section of packages with a foil plane can be any: from triangular to polygonal. The calculations carried out on the obtained electron microscopic images showed that the average transverse size of a separate rail in different packages differs significantly from each other:

- There are packages (Figures 23-24) in which the average size is 0.15 microns;
- whereas in other packages (Figures 25-27) the average size of the rails is 0.50 microns.

Figure 23. Electron microscopic image of the fine structure of the surface of a grade two steel sample after electrolytic plasma surface quenching: packet-plate martensite, the boundary of two grains (P – packet martensite, LLM – Lamellar low–temperature martensite)

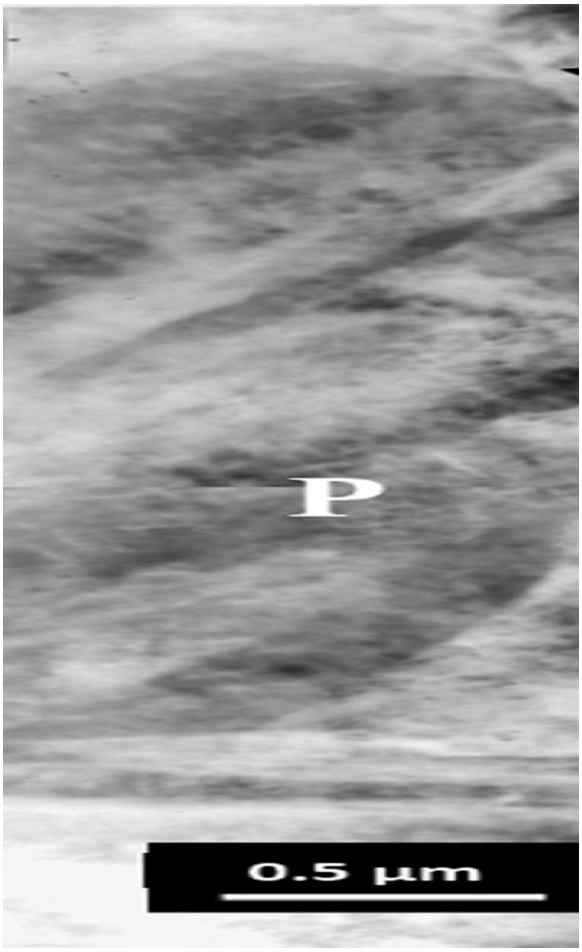

We noted above that in the initial state of steel in fragmented ferrite there are fragments that are sharply different in size: in the center of the grain – large, near the boundaries of "perlite – ferrite" – small. Apparently, packages with narrow slats were formed in sections of material with small fragments, packages with wide slats - in sections of material with large fragments. The fact that the formation of batch martensite occurred from fragmented ferrite is indicated by the fact that the volume fraction of batch martensite, calculated according to the formulas specified in the second section, is 60%, i.e. almost as much as there was fragmented ferrite in the initial state.

Lamellar low-temperature martensite (LLM) is a fairly large, or separately located, martensite crystals (plates) with a dislocation structure (Figure 23), or two or three plates arranged in parallel. According to the calculations, the volume fraction of lamellar low-temperature martensite is 10%. Comparison with the initial state of steel shows that lamellar low-temperature martensite was most likely formed from unfragmented ferrite, the volume fraction of which was also 10%.

Lamellar high–temperature martensite (LHM) is large, separately located martensite crystals (plates), often extending through the entire grain, as well as crystals of arbitrary shape that do not have a clear cut and do not have their own interface boundaries. It is well known that martensitic transformation is almost always incomplete. This leads to the presence of a certain amount of residual austenite (γ-phase) in the material.

The residual austenite (γ-phase) has a face-centered cubic (FCC) crystal lattice and is, like the α-phase, a solid solution based on iron atoms of introduction (C, N, etc.) and substitution (Cr, Ni, Mo, V, etc.) simultaneously. The main nodes, as in the α-phase crystal lattice, are occupied by iron atoms and substitution elements, tetrahedral (mostly) internodes are partially occupied by carbon atoms. The residual austenite (γ-phase) is located in the form of thin layers (~ 20-50 nm) along the boundaries of crystals (rails and plates) of martensite, as well as inside the plates in the form of "needles" or "islands". The crystal lattices of the residual austenite and the α-phase, regardless of the type and location of the residual austenite, are always interconnected by the Kurdyumov-Sachs orientation ratio.

Figure 24. Electron microscopic image of the fine structure of the surface of a grade two steel sample after EPSQ a – is a light–field image; b – is a micro–diffraction pattern; c – is its indexed scheme containing α- and γ-phase reflexes.

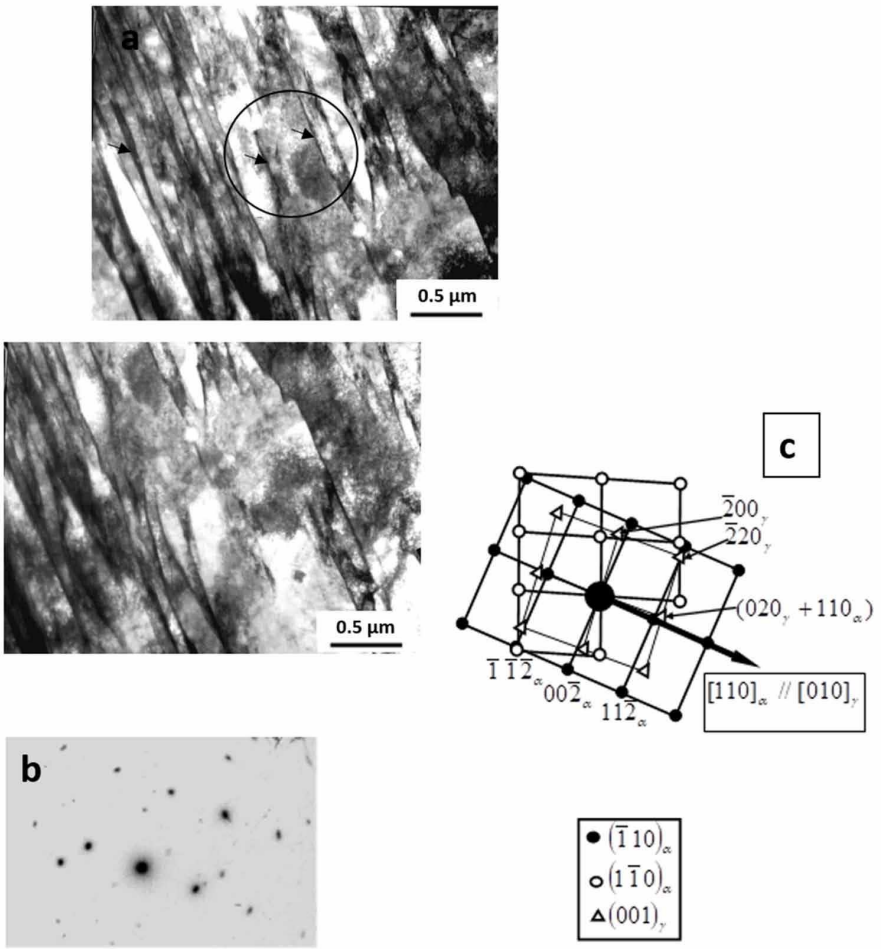

Studies have shown that in grade two steel after surface hardening, residual austenite (γ-phase) in batch martensite is also present at the boundaries of martensitic rails in the form of long thin layers. It should be noted that the γ-phase interlayers are present both in packages with narrow (Figure 24) and wide (Figure 25) slats.

As a confirmation, we will analyze this in more detail using the example of Figure 24. Residual austenite (γ-phase) is present at the boundaries of narrow martensitic slats in the form of thin layers (Figure 24a). The presence of the γ-phase is confirmed by the microdifraction pattern obtained from this site (Figure 24b) and its indexed scheme (Figure 24c). As can be seen from the microdifraction pattern and its indexed scheme, the direction (Tabieva, Popova, Nikonenko, et al, 2020)$_{\alpha}$ coincides with the direction (Balanovskij, 2006)$_{\gamma}$. This is also confirmed by the solution of matrix equations:

$$\text{for planes } \begin{pmatrix} u \\ v \\ w \end{pmatrix}_{\alpha} = \begin{bmatrix} 1 & \bar{1} & 0 \\ 1 & 1 & 0 \\ 0 & 0 & 2 \end{bmatrix} \cdot \begin{pmatrix} 0 \\ 0 \\ 1 \end{pmatrix}_{\gamma} = \left(\bar{1}10\right)_{\alpha};$$

$$\text{for directions } \begin{bmatrix} h \\ k \\ l \end{bmatrix}_{\alpha} = \begin{bmatrix} 1 & \bar{1} & 0 \\ 1 & 1 & 0 \\ 0 & 0 & 1 \end{bmatrix} \cdot \begin{bmatrix} 0 \\ 1 \\ 0 \end{bmatrix}_{\gamma} = \left[110\right]_{\alpha}.$$

Thus, from the solution of matrix equations it turns out: (Tabieva, Popova, Nikonenko, et al, 2020)$_{\alpha}$. (Balanovskij, 2006)$_{\gamma}$ and $(\bar{1}10)_{\alpha}$. $(001)_{\gamma}$, This is observed in the microdifraction pattern (Figure 24b). The black arrow indicates the coinciding directions (Tabieva, Popova, Nikonenko, et al, 2020)$_{\alpha}$ and (Balanovskij, 2006)$_{\gamma}$, with the $\left(\bar{1}10\right)_{\alpha}$ *II* $\left(001\right)_{\gamma}$ – Kurdyumov-Sachs ratio.

Figure 25 shows an electron microscopic image of the fine structure of the surface of a sample of grade two steel after electrolytic-plasma surface hardening obtained on a TEM, which shows laths of packet martensite, and along the borders of laths there are interlayers of residual austenite (γ) with precipitates of special $M_{23}C_6$ carbides. Figure 25 shows a package consisting of a group of wide martensite laths, at the boundaries of which there are interlayers of the γ-phase. The presence of the γ-phase is confirmed by the dark-field image (Figure 25c) obtained in the reflection $[\bar{2}20]$of the γ-phase, the microdiffraction pattern obtained from this area (Figure 25b), and its indicated scheme (Figure 25d). As can be seen from the microdiffraction pattern and its indicated scheme, the direction $[0\bar{2}1]_{\alpha}$ coincides with the direction $[\bar{1}\bar{1}1]_{\gamma}$ (coincident directions in Figure 25d are marked with an arrow).

This is also confirmed by solving the matrix equations:

$$\text{for planes } \begin{pmatrix} u \\ v \\ w \end{pmatrix}_{\alpha} = \begin{bmatrix} 1 & \bar{1} & 0 \\ 1 & 1 & 0 \\ 0 & 0 & 2 \end{bmatrix} \cdot \begin{pmatrix} 1 \\ 1 \\ 2 \end{pmatrix}_{\gamma} = \left(012\right)_{\alpha};$$

Figure 25. Electron microscopic image of the fine structure of the surface of a sample of steel grade two after EPSQ a – bright-field image; b – microdiffraction pattern; c – dark-field image obtained in closely spaced reflections [ ]γ and [ ]C; d – is its indicated scheme

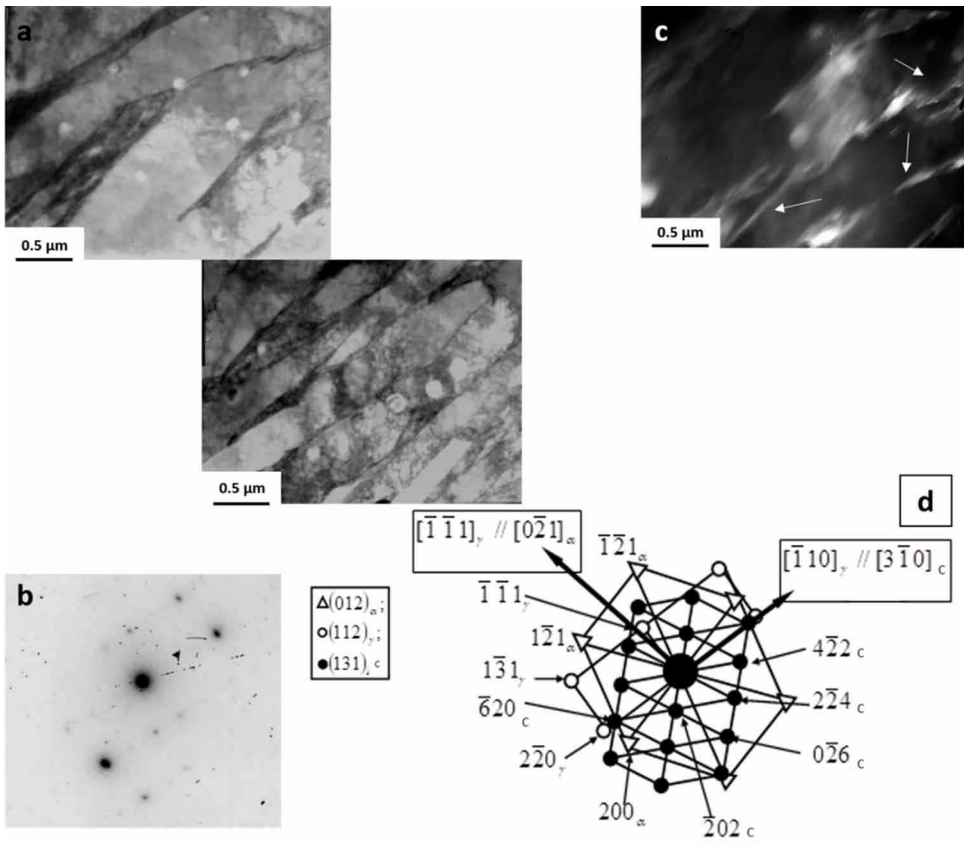

for destinations $\begin{bmatrix} h \\ k \\ l \end{bmatrix}_{\alpha} = \begin{bmatrix} 1 & \bar{1} & 0 \\ 1 & 1 & 0 \\ 0 & 0 & 1 \end{bmatrix} \cdot \begin{bmatrix} \bar{1} \\ \bar{1} \\ 1 \end{bmatrix}_{\gamma} = \left[0\bar{2}1\right]_{\alpha}$.

Thus, from the solution of matrix equations it turns out: $(012)_{\alpha}$. $(112)_{\gamma}$ and $[0\bar{2}1]_{\alpha} \,//\, /[\bar{1}\,\bar{1}1]_{\gamma}$, which is observed in the microdiffraction pattern (Figure 25b) and indicated scheme (Figure 25d).

In Figure 25, the arrows indicate:

1) coinciding directions $[\,\bar{1}10\,]_{\gamma}$ and $[\,3\bar{1}0\,]_{K}$, which means $[\bar{1}10]_{\gamma} \,//\, /\, [3\bar{1}0]_{K}$, at the same time $\left(112\right)_{\gamma}$ *II* $\left(131\right)_{K}$ - the ratio "cube-cube";
2) coinciding directions $[\,0\bar{2}1\,]_{\alpha}$ and $[\,\bar{1}\,\bar{1}1\,]_{\gamma}$, which means $[0\bar{2}1]_{\alpha} \,//\, /\, [\bar{1}\,\bar{1}1]_{\gamma}$, at the same time $(012)_{\alpha} \,//\, /\, (112)_{\gamma}$) – Kurdyumov-Sachs ratio. In the diagram (d), the letter "K" denotes $M_{23}C_6$ carbide. In (c), white arrows mark interlayers of the γ-phase containing carbide particles.

Thus, the presented figures 24 and 25 indicate that residual austenite is present at the boundaries of all laths, regardless of their size. The volume fraction of retained austenite (γ-phase) in packet martensite is 6.5%.

An electron microscopic image of the fine structure of the surface of a sample of steel grade two after electrolytic-plasma hardening of the surface showed that along the boundaries of laths of packet martensite there are interlayers of residual austenite, which are marked with black arrows in Figures 26a and 27a. Inside the laths of packaged martensite, there are particles of cementite which are marked with white arrows in Figure 26a.

It was also revealed that there are reflections belonging to the α- and γ-phases, and carbides: cementite and carbides of a special type $M_{23}C_6$ that are in the γ-phase, marked with the letter "K" on the indicated scheme (Figure 27c) of the obtained microdiffraction pattern (Figure 27b) the area shown in Figure 27a.

Figure 26. Electron microscopic image of the fine structure of the surface of a sample of steel grade two after EPSQ a – bright-field image; b – microdiffraction pattern; c – its indicated scheme containing reflections of the α- and γ-phases

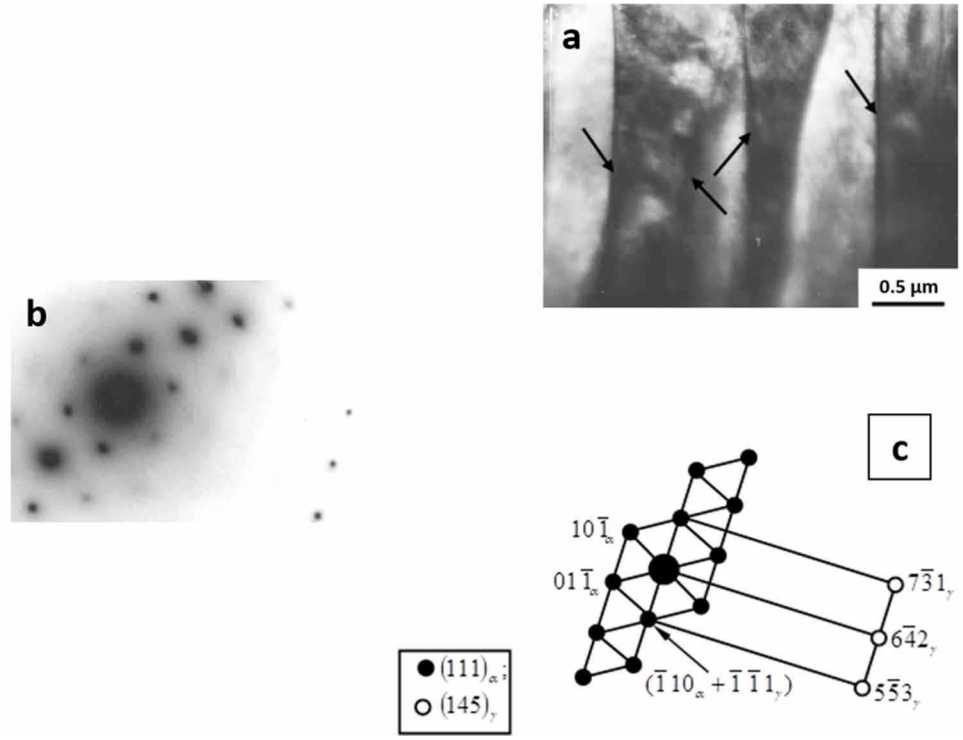

The volume fraction of the γ-phase in lamellar low-temperature martensite at the plate boundaries is 2%, inside the plates – 5.7%. In all martensite crystals, cementite particles are thin elongated plates (needles) located in two and three directions relative to the axis of the martensite crystal. The average particle size in martensitic slats is 12 × 40 nm, in plates of low–temperature martensite – 16 × 80 nm, in plates of high-temperature martensite - 32 × 84 nm. This means that the smallest particles of cementite

are formed in the batch "self-released" martensite, the largest – in the lamellar high-temperature. Note that the distribution density of cementite particles in batch and lamellar low-temperature martensite is the same and higher than in lamellar high-temperature martensite, i.e. the distance between cementite particles in batch and lamellar low-temperature martensite (r = 100 nm) is less than in lamellar high-temperature (r = 140 nm) martensite.

The calculations performed showed that the volume fraction of cementite in batch (rack) martensite is 0.27%, in low–temperature lamellar – 0.95%, in high-temperature lamellar - 2%. Thus, the electrolyte-plasma surface hardening of grade two steel led not only to martensitic transformation, but also to the "self-release" of steel. The conducted studies have shown that in addition to cementite, there are also particles of carbides of a special type $M_{23}C_6$ in the structure of steel (Tabieva, Uazyrhanova, Popova, et al, 2020).

Carbides of the $M_{23}C_6$ type have a cubic crystal lattice (space group Fd3m). The unit cell of this carbide contains more than 100 atoms occupying various non-equivalent positions. Such carbides include Fe_4Mo_2C, $Fe_6Mo_6C_6$, $Fe_{21}Mo_2C_6$, $Fe_{21}Cr_2C_6$. These carbides are found at the boundaries of martensitic

Figure 27. Electron microscopic image of the fine structure of the surface of a sample of steel grade two after EPSQ a – bright-field image; b – microdiffraction pattern of area (a); c – its indicated scheme

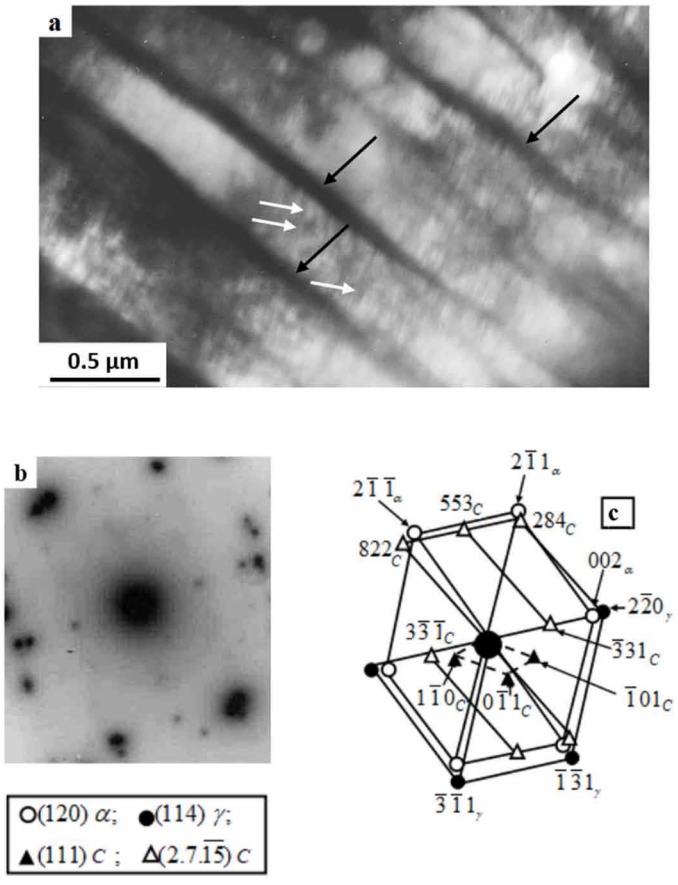

lath, as well as inside plates of low-temperature and high-temperature martensite. Microdifraction patterns and their indexed schemes obtained from these sites serve as proof of their presence. Let's explain this in more detail.

We noted above that surface hardening led to the "self-release" of steel, which is similar to ordinary tempering. It is well known that tempering of hardened steels leads to three main processes:

1) to the evolution of the defective structure, which consists in such a restructuring of the defective structure in which the internal stress fields decrease;
2) to reduce the density of defects and the energy of the defective structure;
3) to the decomposition of a solid solution with the formation of particles of carbide phases.

Due to the strong interaction of dislocations, sub-boundaries and carbon atoms, these processes are interconnected.

In addition, the "self-release" of steel means that the decomposition of the solid solution in the α- and γ-phases already begins during the surface quenching process and during the "self-release" a diffusion γ ® α transformation already begins to occur with the release of special type carbide particles (in particular, $M_{23}C_6$).

The evolution of the defective structure of steel during "self-release" and especially the change in its quantitative parameters have not been investigated in previously published works. Only a change in the phase composition of the hardened steel was noted, i.e. the presence of cementite (Ababkov, et al., 2021; Abuali Galedari, & Mousavi Khoei, 2013; Lee & Polycarpou, 2005; Zhang, 2002; Zhang, 2002; Zhang, 2002).

Based on the conducted studies, it can be argued that $M_{23}C_6$ carbide particles located at the boundaries of martensitic crystals are isolated from the γ-phase. The proof of this is that they are observed inside the layers of residual austenite: in microdifraction patterns obtained from the boundaries of martensitic crystals (see Figures 24b, 27b), along with $M_{23}C_6$ phase reflexes, γ-phase reflexes are always present.

The feasibility of this ratio is confirmed by the indexing of microdifraction patterns obtained from such sections of the structure (Figure 25). The particles of carbides $M_{23}C_6$, located in the layers of residual austenite, have a rounded shape. Their average size, regardless of the location of the particle, is ~ 5 nm. Due to the small size of the particles, they are detected only on dark-field images and at high magnification. However, they are reliably detected by microdifraction patterns when they are indexed.

In the near-surface zone of the grade two steel sample, after surface quenching, $M_{23}C_6$ carbide particles unrelated to the γ-phase were also found. These are particles with a rounded shape, the average size of which is ~ 80 nm. They were found in plates of high-temperature martensite on dislocations of the α-phase.

Thus, it can be argued that the release of special carbides of the $M_{23}C_6$ phase is due to:

- The decay of residual austenite and martensite,
- Partial dissolution of cementite,
- The departure of carbon from dislocations and crystal boundaries of the α-phase.

That is, in all cases, carbon from residual austenite, α-solid solution, cementite particles and crystal lattice defects goes to the formation of special carbides.

It should be noted that the intensity of the processes of decomposition of solid solutions of α and γ and the formation of a carbide phase in various structural components of the α-phase (in batch martensite, inside plates of low-temperature and high-temperature martensite) is different. It is also different within each structural component. It depends on many factors. Such factors, in particular, include the state of the source material (including the degree of fragmentation of the material, the type of fragments formed).

The calculations performed showed that the volume fraction of $M_{23}C_6$ carbides in lamellar high-temperature martensite is 2.7%. It should be noted that due to the small size of the $M_{23}C_6$ particles in the γ-phase, their volume fraction in each structural component of martensite does not exceed 0.01% and therefore is not taken into account in quantitative calculations in the future.

Thus, electrolytic plasma surface hardening of grade two steel in the near-surface zone of the sample resulted in:

1) to martensitic transformation;
2) to the "self-release" of steel;
3) to a diffusive γ ® α transformation with the release of carbide particles of a special type $M_{23}C_6$.

4.5 Quantitative Parameters of the Structural-Phase State of Grade Two Steel After Surface Quenching

Based on the conducted studies, it can be argued that in the near-surface zone of the grade two steel sample after the EPSQ, the quantitative phase composition in each structural component of martensite and in general for the material has the form shown in Table 5.

Table 5. Phase composition of grade two steel in the near-surface zone after electrolyte-plasma surface quenching

Phase Composition Parameters		Morphological Components of Martensite			In General, According to the Material
		Batch Martensite	Lamellar Martensite		
			Low Temperature	High Temperature	
Volume fraction (P_V)		60%	10%	30%	100%
Fraction γ-phases	at the borders	6.5%	2%	0	4.1%
	inside	0	5.7%	8.5%	3.1%
	sum	6.5%	7.7%	8.5%	7.2%
Cementite	δ_C	0.27%	0.95%	2.0%	0.86%
	dimensions, nm	12 × 40	16 × 80	32 × 84	18 × 60
	r, nm	100	100	140	110
$M_{23}C_6$ Carbides	δ_K	0	0	2.7%	0.8%
	dimensions, nm	–	–	80	80
	r, nm	–	–	240	70

Table 6. Average quantitative parameters of fine structure in batch, lamellar low-temperature and high-temperature martensite, as well as in general for the material in grade two steel after EPSQ

Morphological Component	Average Quantitative Parameters of Fine Structure					
	P_V	ρ, cm^{-2}	$\rho_{\pm}$, cm^{-2}	χ, cm^{-1}	σ_{Sh}, MPa	σ_{∂}, MPa
Batch martensite	60%	3.31×10^{10}	2.60×10^{10}	650	365	320
Lamellar low-temperature martensite	10%	2.52×10^{10}	1.86×10^{10}	465	315	270
Lamellar high-temperature martensite	30%	2.33×10^{10}	1.64×10^{10}	410	305	255
In general, according to the material	100%	2.94×10^{10}	2.24×10^{10}	560	340	295

The dislocation structure, as can be seen from the figures presented above, represents dense dislocation grids in all structural components of martensite. The calculations performed showed that in batch martensite the average scalar dislocation density is 3.31×10^{10} cm^{-2}, in plate low-temperature martensite the value of ρ is slightly lower and is equal to 2.52×10^{10} cm^{-2}, in plate high-temperature martensite the value of ρ is even lower (2.33×10^{10} cm^{-2}).

The dislocation structure in all structural components of martensite is polarized. This is indicated by the presence of flexural extinction contours in all martensitic crystals. For each morphological component (in batch, lamellar low-temperature and high-temperature martensite), as well as for the whole material in the near-surface zone of the grade two steel sample after surface quenching, the following quantitative parameters of the fine structure χ, $\rho_{\pm}$, σ_{∂} and σ_{Sh} were calculated according to the data ρ and the dimensions of the bending extinction contours, the average values of which presented in Table 6.

As can be seen from the calculations performed on the surface data of samples after EPSQ, the results of which are shown in Table 6:

- The highest quantitative parameters were found in batch martensite, the lowest – in lamellar high-temperature martensite.
- The conditions are met in all the material: $\rho > \rho_{\pm}$ and $\sigma_{Sh} > \sigma_{\partial}$. This means that the bending-torsion (distortion) of the crystal lattice of grade two steel in the near-surface zone of the sample after surface hardening is purely plastic in nature, which will not lead to the formation of microcracks in the material.

Conclusions on the Section

Thus, based on the analysis of the obtained results of studies of grade two wheel steel before and after electrolyte-plasma surface hardening, the following conclusions can be drawn:

1. The conducted studies on a transmission electron microscope have shown that, in the initial state, grade two steel:
   - Ferrite is present in the form of unfragmented and fragmented, with volume fractions of ~10% and ~55%. The volume fraction of lamellar perlite in the volume of the material is 35%;
   - The calculations performed showed that the average scalar density of dislocations in pearlite plates is equal to 2.1×10^{10} cm^{-2}, unfragmented and fragmented ferrite, as in perlite, is represented by dislocation grids, the average scalar density of dislocations is 2.57×10^{10} cm^{-2} and 2.89×10^{10} cm^{-2} ;
   - The boundaries of the fragments are free of carbides, the carbide phase is also not detected inside the fragments, the average size of fragments of fragmented ferrite is ~ 1 microns;
   - The conditions are met in all the material: $\rho > \rho_{\pm}$ and $\sigma_{Sh} > \sigma_{\partial}$. The bending-torsion (distortion) of the crystal lattice of the grade two wheel steel in its initial state is purely plastic in nature, which does not lead to the formation of microcracks in the material.
2. The conducted electrolyte-plasma surface hardening led to:
   - Formation of batch-plate martensite, as well as the presence of reflexes belonging to the α- and γ-phases, and carbides: cementite and carbides of a special type $M_{23}C_6$ in the γ-phase.
   - The presence of residual austenite (γ-phase) in the batch martensite at the boundaries of martensitic rails in the form of long thin layers. The volume fraction of residual austenite (γ-phase) in batch martensite is 6.5%.
   - Formation of particles of $M_{23}C_6$ carbides not associated with the γ-phase, having a rounded shape, an average size of ~80 nm, found in plates of high-temperature martensite on dislocations of the α-phase.
   - In lamellar low-temperature martensite, the volume fraction of the γ-phase at the plate boundaries is 2%, inside the plates – 5.7%. The volume fraction of lamellar low-temperature martensite is 10%, residual austenite is present not only at the plate boundaries in the form of long thin layers, but also inside the plates in the form of "needles" or twin-type colonies.
   - In lamellar high-temperature martensite, residual austenite is present only inside the plates in the form of "needles" or twin-type colonies, the volume fraction of the γ-phase in lamellar high-temperature martensite is 8.5%, the volume fraction of $M_{23}C_6$ carbides in lamellar high-temperature martensite is 2.7%;
3. The results of studies of electron microscopic pictures showed that:
   - The average size of cementite particles in martensitic slats is 12×40 nm, in plates of low–temperature martensite – 16×80 nm, in plates of high-temperature martensite - 32×84 nm. The volume fraction of cementite in batch (rack) martensite is 0.27%, in low–temperature lamellar – 0.95%, in high-temperature lamellar - 2%.
   - Bending-torsion (distortion) of the crystal lattice of grade two steel after surface hardening is purely plastic in nature, which will not lead to the formation of microcracks in the material, since the following conditions are met in the entire material: $\rho > \rho_{\pm}$ and $\sigma_{Sh} > \sigma_{\partial}$.

CONCLUSION

In this work, the structural-phase states, tribological and mechanical properties, features of the formation of the fine structure of grade two wheel steel before and after electrolytic-plasma surface hardening were studied, and the volume fractions of structural-morphological components, particles of the second phases, scalar excess dislocation densities were quantified, which allow us to formulate the following conclusions:

1. A method and an optimal mode of electrolyte-plasma surface hardening of the material of a railway bandage made of grade two wheel steel has been developed, providing a modified layer with a thickness of 1000-1500 microns with increased hardness and wear resistance due to the formation of a fragmented structure of packet-plate martensite and carbide particles of the second phases.
2. By transmission electron microscopy, it was found that:
    - in the initial state, grade two steel consists of a α-phase: ferrite is present in the form of unfragmented and fragmented, with volume fractions of ~ 10% and ~ 55%, respectively. The volume fraction of lamellar perlite is 35% in the volume of the material. The boundaries of the fragments are free of carbides, the carbide phase is also not detected inside the fragments, the average size of fragments of fragmented ferrite is ~ 1 microns.
    - electrolyte-plasma surface hardening of grade two steel leads to the formation of a batch-plate martensite with carbides of a special type $M_{23}C_6$, which are in the γ-phase. The release of special carbides $M_{23}C_6$ is due to the decay of residual austenite and martensite, partial dissolution of cementite, and the departure of carbon from dislocations and crystal boundaries of the α-phase.
    - the volume fractions of batch, lamellar low-temperature and lamellar high-temperature martensite are ~ 60%, ~ 10% and ~ 30%, respectively. It is shown that in lamellar high-temperature martensite, residual austenite is present only inside the plates in the form of "needles" or twin-type colonies with an average volume fraction of 8.5%.
3. The dislocation structure of grade two steel was studied before and after electrolytic plasma surface quenching. It is established that:
    - in the initial state, both in ferrite and perlite, the dislocation structure is polarized. This is indicated by the presence of flexural extinction contours throughout the material. Calculations of the average scalar dislocation density in pearlite plates, which are 2.1×10^{10} cm^{-2}, in unfragmented and fragmented ferrite – 2.57×10^{10} cm^{-2} and 2.89×10^{10} cm^{-2}, respectively, were performed;
    - after electrolytic-plasma surface hardening of grade two steel, the dislocation structure in all structural components of martensite is polarized, as indicated by the presence of flexural extinction contours in all martensite crystals. The calculations performed for the first time showed that in batch martensite the average scalar dislocation density is 3.31×10^{10} cm^{-2}, in lamellar low-temperature martensite and lamellar high-temperature martensite is equal to 2.52×10^{10} cm^{-2} and 2.33×10^{10} cm^{-2}, respectively.

The development of promising technologies aimed at improving traditional and creating new methods of impact on the surface to give it the properties required by operating conditions is undoubtedly one of the urgent tasks of modern science and technology. This method is characterized by lower energy

consumption, simplicity of technological equipment, and large dimensions of the hardened zone. The advantages of the method are a rather high productivity of the process and the ability to harden parts of large mass and complex profile. Thus, the studies performed show that the developed method of electrolytic-plasma surface hardening of steels in an aqueous electrolyte solution leads to changes in the structural-phase state of the surface layers and the formation of hardening phases in order to obtain products with increased mechanical and tribological characteristics.

ACKNOWLEDGMENT

In conclusion, the author expresses his great gratitude:

To the team of LLP Plasma Science for the opportunity and support provided when performing experimental and analytical work.

To the staff of the Scientific Research Center "Surface Engineering and Tribology" for the opportunity to participate in the research and support provided in the performance of experimental and analytical work.

To the staff of the laboratory of Tomsk State University of Architecture and Civil Engineering for assistance in conducting research on a transmission electron microscope.

To the management and employees of the D.Serikbayev East Kazakhstan Technical University for the opportunity and support provided.

REFERENCES

Ababkov, N., Smirnov, A., Danilov, V., Popova, N., & Nikonenko, E. (2021). Structural-phase state, mechanical properties, acoustic and magnetic characteristics in the sustainable deformation localization zones of power equipment made of structural and heat resistant steels. *Metals, 11*(10), 1638.

Abuali Galedari, S., Mousavi Khoei, S.M. (2013). Effect of pulse frequency on microstructure and surface properties of Ck45 steel treated by plasma electrolysis method. *Journal of Alloys and Compounds, 551*, 415-421.

Balanovskii, A.E. (2016). Visualization of the process of metal heating and melting in the anode zone in an arc discharge with a tungsten electrode. *High Temperature, 54*, 627-631.

Balanovskij, A.E. (2006). Plazmennoe poverhnostnoe uprochnenie metallov. *Irkutsk: Izdatelstvo IrGTU*, 180.

Balanovskij, A.E. (2015). Ocenka zerna austenita pri plazmennom poverhnostnom uprochnenii sredneuglerodistyh stalej. *Uprochnyayushie tehnologii i pokrytiya, 6*, 27-32.

Balanovskij, A.E. (2016). Osnovnye voprosy teorii plazmennogo poverhnostnogo uprochneniya metallov (Obzor. Chast 3). *Uprochnyayushie tehnologii i pokrytiya, 2,* 20-30.

Balanovskij, A.E. (2006). Rezultaty vnedreniya tehnologii plazmennogo uprochneniya na VSZhD. *Zheleznodorozhnyj transport, 4,* 28-32.

Balanovskij, A.E. (2015). Osnovnye voprosy teorii plazmennogo poverhnostnogo uprochneniya metallov (Obzor. Chast 1). *Uprochnyayushie tehnologii i pokrytiya, 12,* 18-30.

Balanovskij A.E. (2016). Osnovnye voprosy teorii plazmennogo poverhnostnogo uprochneniya metallov (Obzor. Chast 2). *Uprochnyayushie tehnologii i pokrytiya, 1*, 25-34.

Balanovskij, A.E. (2016). Vizualizaciya processa nagreva i plavleniya metalla v anodnoj oblasti pri dugovom razryade s neplavyashimsya elektrodom. *Teplofizika vysokih temperature, 54*, 1-8.

Balanovskij, A.E. (2016). Vozmozhnosti cifrovoj vizualizacii processa nagreva i plavleniya metalla pri dugovom razryade s neplavyashimsya elektrodom. *Svarochnoe proizvodstvo, 6,* 31-39.

Balanovskij, A.E., & Grechneva, M.V., Vu Van, G. (2015). Issledovanie struktury relsovoj stali posle plazmennogo poverhnostnogo uprochneniya. *Uprochnyayushie tehnologii i pokrytiya, 11*, 23-32.

Balanovskij, A.E., & Nesterenko, H.A. (1992). Plazmennoe ciklicheskoe uprochnenie stalej. *Svarochnoe proizvodstvo, 11,* 19-20.

Balanovskij, A.E. & Pletnikov, I.A. (1999). Kompleksnaya ocenka kachestva tehnologii plazmennogo poverhnostnogo uprochneniya bandazhej lokomotivov. *Svarka i diagnostika, 3,* 45-50.

Balanovskij, A.E., & Pletnikov, I.A. (1999). Kompleksnaya ocenka kachestva tehnologii plazmennogo poverhnostnogo uprochneniya bandazhej lokomotivov. Chast 2. *Svarka i diagnostika, 4,* 46-50.

Balanovskij, A.E., & Pletnikov, I.A. (1999). Plazmennoe poverhnostnoe uprochnenie specialnyh stalej. *Metallurgiya mashinostroeniya, 5,* 24-30.

Baranova, L.V., & Demina, E.L. (1986). *Metallograficheskoe travlenie metallov i splavov*. Spravochnik.

Bayatanova, L.B. (2014). *Formirovanie modificirovannyh sloev na poverhnosti nizkouglerodistoj stali metodom vozdejstviya elektrolitnoj plazmoj: dissertaciya na soiskanie uchenoj stepeni doktora filosofii*. Vostochno-Kazahstanskij gosudarstvennyj tehnicheskij universitet im. D.Serikbaeva.

Bayatanova, L.B., Sapataev, E.E., & Tleukenov E.O. (2012). Uprochnenie poverhnosti podshipnikovoj dorozhki burovogo instrumenta elektrolitno-plazmennoj obrabotkoj. *Materialy III Mezhdunarodnoj nauchno-prakticheskoj konferencii s elementami nauchnoj shkoly dlya molodyh uchenyh «Innovacionnye tehnologii i ekonomika v mashinostroenii*. YuTI TPU.

Belkin, P.N. (2005). *Elektrohimiko-termicheskaya obrabotka metallov i splavov*. P. N. Belkin *Mir*.

Belkin, P.N. (2005). Stacionarnaya temperatura anoda, nagrevaemogo v vodnyh elektrolitah / P. N. Belkin, A. B. Belihov, *Inzhenerno-fizicheskij zhurnal*, *75*(6), 19-24.

Berdnikov, A.A., Filippov, M.A., & Studenok, E.S. (2007). Struktura zakalennyh uglerodistyh stalej posle plazmennogo poverhnostnogo nagreva. *Metallovedenie i termicheskaya obrabotka metallov*, *6,* 2-4.

Chudina O.V. (2003). Kombinirovannye metody poverhnostnogo uprochneniya stalej s primeneniem lazernogo nagreva. *Teoriya i tehnologiya*. M.: Izdatelstvo MADI (GTU).

Colm, G. (n.d.). Simplified diagram of a transmission electron microscope. Drawing by Graham Colm, courtesy of Wikimedia Commons. https://www.ccber.ucsb.edu/ucsb-natural-history-collections-botanical-plantanatomy / transmission-electron-microscope.

Dunleavy C.S., Golosnoy I.O., Curran J.A., Clyne T.W. (2009). Characterisation of discharge events during plasma electrolytic oxidation. *Surface & Coatings Technology, 203*, 3410-3419.

Duradzhi V. N., Parsadanyan A. S. (1988). *Nagrev v elektrolite*. Kishinev: Shtinca.

Dyachenko, S. S. (1981). *Formation of austenite in carbon alloys. M*. Metallurgy.

Erkinbekkyzy T.E., Zhurerova L.G, Daryn B. (2020). Influence of electrolyte-plasma hardening technological parameters on the structure and properties of banding steel 2. *Key Engineering Materials, 839*.

Glagolev, A. A. (1941). Geometricheskie metody kolichestvennogo analiza agregatov pod mikroskopom. Lvov: Gosgeolizdat.

Gorelik, S.S., Skakov, Y.A., & Rastorguev, L.N. (2002). *Rentgenograficheskij i elektronno-opticheskij analiz.* M.: MISIS.

Grechneva, M. V. (1992). Plasma hardening of metals in liquid media. Welding, 7, 18–22.

Grechneva, M.V. (1992). Plazmennoe uprochnenie metallov v zhidkih sredah. *Svarochnoe proizvodstvo, 7,* 8-12.

Grechneva, M. V. (2017). Kratkij analiz sostoyaniya tehnologij plazmennogo poverhnostnogo uprochneniya stalej i splavov v RF. *International conference on modern researches in science and technology. Conference Proceedings*. Scientific public organization.

Grigoriants, A.G., Safonov, A.N. (1987). *Methods of surface laser treatment*. Higher School Publ.

Gulyaev, A. P. (1986). *Metallurgy. M*. Metallurgy.

Ivanov, Y.F., Gromov, V.E., & Vorobev, S.V. (2011). Fazovyj sostav i defektnaya substruktura stali 20H13, obrabotannoj elektronnym puchkom v rezhime oplavleniya poverhnosti. *Fundamentalnye problemy sovremennogo materialovedeniya*.

Ivanov, Y.F. & Kozlov, E.V. (1991). Electron microscopic analysis of the martensitic phase of steel 38KHN3MFA. *Ferrous metallurgy, 8,* 38-41.

Ivanov Yu.F., Kozlov E.V. (2002). Volumetric and surface hardening of structural steel morphological analysis of the structure. Physics. - 2002. No. 3. pp. 5-23.

Jin, X., Wang, B., Xue, W., Du, J., Wu, X., & Wu, J. (2013). Characterization of wear-resistant coatings on 304 stainless steel fabricated by 148 cathodic plasma electrolytic oxidation. *Surface & Coatings Technology, 236*, 22-28.

Kidin I.N. (1978). Elektrohimiko-termicheskaya obrabotka metallov i splavov Tekst. *Metallurgiya*, 320.

Ko, Y., Lee, K., & Shin, D. (2013). Effect of ammonium metavanadate on surface characteristics of oxide layer formed on Mg alloy via plasma electrolytic oxidation. *Surface & Coatings Technology, 236*, 70-74.

Kondrat'ev V.V., Balanovskii A.E., Ivanov N.A., Ershov V.A., Kornyakov M.V. (2014). Evaluation of the Effect of Modifier Composition with Nanostructured Additives on Grey Cast Iron Properties. *Metallurgist, 58,* 377-387.

Kong, J. H., Takeda, T., Okumiya, M., Tsunekawa, Y., Yoshid, M., & Kim, S. G. (2012). The Study about Surface Modification of Steel by Water Plasma. *Proc. of 13th International Conference on Plasma Surface Engineering*, Garmisch-Partenkirchen.

Korotkov, V.A. (2016). The 15th Anniversary of the Manual Plasma Quenching. Ferrous Metallurgy. *Bulletin of Scientific, Technical and Economic Information*, *10*, 62-68.

Korotkov, V.A., Baskakov, L.B., & Tolstov, I.A. (1991). Vosstanovitelnaya naplavka i uprochnenie rolikov rolgangov. *Svarochnoe proizvodstvo, 3*, 31-33.

Kozlov, E., Skakov, M., Uazyrkhanova, G., & Popova N. (2014). Redistribution of second phase particles in surface layers of deformed roll. *Advanced Materials Research, 1013*, 158-165.

Kozlov, E.V., Popova, N.A., & Koneva, N.A. (2004). Fragmented substructure formed in BCC steels during deformation. *RAS. The series is physical*, *68*(10), 1419-1428.

Kulikov, I.S., Vashenko, S.V., & Kamenev A.Ya. (2010). *Elektrolitno-plazmennaya obrabotka materialov.* Minsk: Belarus.navuka.

Lahtin Y.M., & Arzamasov B.N. (1985). *Himiko-termicheskaya obrabotka metallov: uchebnoe posobie dlya vuzov.* M.: Metallurgiya.

Lakhtin Y.M., & Arzamasov B.N. (1985). *Chemical and thermal treatment of metals*. Metallurgy Publ.

Lee K.M., & Polycarpou A.A. (2005). Wear of conventional pearlitic and improved bainitic rail steels. *Wear, 259*, 391-399.

Leshchinsky L. K., & Samotugin S. S. (2001). *Mechanical properties of plasma-hardened 5% chromium tool steel deposited by arc welding. Welding,* 25-30.

Leshinskij, L. K., Samotugin, S. S., Pirch, I. I., & Komar, V. I. (1990). Plazmennoe poverhnostnoe uprochnenie. Kiev: Tehnika.

Majorov, V. S. (2009). *Lazernoe uprochnenie metallov. V kn.: Lazernye tehnologii obrabotki materialov: sovremennye problemy fundamentalnyh issledovanij i prikladnyh razrabotok.* M. Fizmatlit.

Majorov V.S. (2009). *Lazernye tehnologii obrabotki materialov: sovremennye problemy fundamentalnyh issledovanij i prikladnyh razrabotok*. M.: Fizmatlit.

Makarov A.V. (2009). Povyshenie iznosostojkosti splavov zheleza za schet sozdaniya metastabilnyh i nanokristallicheskih struktur: avtoref. …dokt.teh.nauk. *Institut mashinovedeniya Uralskogo otdeleniya RAN*. Chelyabinsk.

Malinovskaya V.A. (2006). *Raspredelenie azota i ugleroda, fazovaya struktura gradientnyh sloev i mehanicheskie svojstva stali 20H2N4A posle nitrocementacii: dis… kand. tehn*. Tomsk.

Martin, J., Melhem, A., Shchedrina, I., Duchanoy, T., Nominé, A., Henrion, G., Czerwiec, T., & Belmonte T. (2013). Effects of electrical parameters on plasma electrolytic oxidation. *Surface & Coatings Technology*, *221*.

Medvedev, S.I., Nezhivlyak, A.E., Grechneva, M.V., Balanovsky, A.E., & Ivakin, V.L. (2015). Optimization of plasma hardening conditions of the side surface of rails in PUR-1 experimental equipment. *Welding International, 29,* 643-649.

Medvedovskaya L. A., & Shur N. F. (1983). Oborudovanie i tehnologiya lazernoj termicheskoj obrabotki (obzor). *Metallovedenie i term*.

Menin, R., Ramos, E., & Magrini, M. (1981). Laser surface treatment of carbon and alloy steels. *Proc. 4 Inter. conf. of rapid quench. metals*. Sendai.

Moon, S., & Jeong, Y. (2009). Generation mechanism of microdischarges during plasma electrolytic oxidation of Al in aqueous solutions. *Corrosion Science, 51*, 1506-1512.

Nesterov, D.K., & Sapozhkov, V.E. (1989). i dr. Uprochnenie relsov iz zaevtektoidnoj stali kombinirovannoj termoobrabotkoj. *MiTom, 12*, 2-5.

Patent na poleznuyu model Nº 5365 Sposob uprochneniya zheleznodorozhnyh koles. Data registracii v Gosudarstvennom reestre poleznyh modelej Respubliki Kazahstan.

Paulmier, T., Bell, J.M., Fredericks, P.M. (2008). Development of a novel cathodic plasma-electrolytic deposition technique. Part 2: Physico-chemical analysis of the plasma discharge. *Journal of materials processing technology, 208,* 117-123.

Pogrebnjak, A. D., & Tyurin, Yu. (2000). Preparation and investigation of the structure and properties of Al_2O_3 plasma-detonation coatings. *Techn. Phys. Lett., 26*(11), 960-964.

Pogrebnjak, A. D., Tyurin, Y. N., & Kobzev, A. P. (2003). Mass transfer and doping during electrolyte-plasma treatment of cast iron. *Tech. Phys. Lett., 29*(4), 312-315.

Poletika, I.M., Golkovskij, M.G., & Perovskaya, M.B. (2006). Elektronno-luchevaya zakalka poverhnostnogo sloya stali vne vakuuma. *Fizicheskaya mezomehanika, 9,* 181-184.

Polyak M.S. (1995). Tehnologiya uprochneniya. *Tehnologicheskie metody uprochneniya: spravochnik v 2 t.* Mashinostroenie.

Popova, N.A., Nikonenko, E.L, Tabieva, E.E., & Uazyrkhanova, G.K. (2020). Structure and phase composition of ferritic-perlitic steel surface after electrolytic plasma quenching. *Russian Physics Journal, 63*(5), 791-796.

Rahadilov, B.K. (2014). *Elektrolitno-plazmennoe azotirovanie poverhnostnyh sloev bystrorezhushih stalej: dissertaciya na soiskanie uchenoj stepeni doktora filosofii* [Dissertation, Vostochno-Kazahstanskij gosudarstvennyj tehnicheskij universitet im. D.Serikbaeva].

Rakhadilov, B.K., Tabiyeva, Y.Y., Uazyrkhanova, G.K., Zhurerova, L.G., & Baizhan, D. (2020). Inñuence of electrolytic-plasma surface quenching on the structure and strength properties of ferritic-pearlite class wheel steel. *Eurasian Journal of Physics and Functional Materials, 4*, 167-173.

Rakhadilov, B.K., Tabiyeva, Y.Y., Uazyrkhanova, G.K., Zhurerova, L.G., Maulit, A., & Baizhan, D. (2019). Surface modification of steel mark 2 electrolytic-plasma exposure. *Eurasian Journal of Physics and Functional Materials, 3*, 355-362.

Rakhadilov, B.K., Tabiyeva, Y.Y., Uazyrkhanova, G.K., Zhurerova, L.G., & Popova N.A. (2020). Effect of electrolyte-plasma surface hardening on structure wheel steel 2. *Bulletin of Karaganda State University, 2* (98), 68-74.

Richard, R. (2007). *Track Demonstration of Laser-Treated Rail to Reduce Friction and WearTransportation Technology Center / R*. Richard. Inc.

Sadovsky, V. D., & Malyshev, K. A. (1984). *Phase and structural transformations during heating of steel*. Metallurgizdat.

Saltykov S.A. (1976). Stereometricheskaya metallografiya. *Metallurgiya*.

Samotugin, S.S., Muratov, V.A, & Kovalchuk, A.V. (1997). Plazmennoe uprochnenie instrumentov kolcevoj formy. *Metallovedenie i termicheskaya obrabotka metallov*.

Skakov, M., Bayatanova, L., & Sheffler, M. (2012). The drilling tool electrolyte-plasma material hardening technology planning and research. *The 7th International Forum on Strategic Technology*. Tomsk.

Skakov, M., Kurbanbekov, S., Tabieva, Y., & Zamanbekuly, E. (2013). Nitriding and carbonitriding influence on stainless steels surface layers changes. *Applied Mechanics and Materials, 379*, 105-109.

Skakov, M., & Rakhadilov, B. (2012). Change of structure and wear-resistance of P6M5 steel for processing in electrolyte plasma. *32th All-Polish Tribology conference Autumnal school of Tribology 2012*. Wroclaw University of Technology Institute of Machine Design and Operation.

Skakov, M.K., Bayatanova, L.B., & Scheffler, M. (2013). Changes of Structural-Phase Condition In *18CrNi3MoA-Sh Steel After Elektrolyte-Plasma Processing*. Advanced Materials Research.

Skakov, M.K., Bayatanova, L.B., & Scheffler, M. (2012). *Research of Surface Treatment on the Microstructure, Microhardness and Wear Resistance of 18CrNi3MoA-Sh Steel*. Tribologia.

Skripkin, A.A., Necvetaev, V.A., Sherbakov, V.E., & Minenko, N.Y. (1992). Poluchenie teplostojkih sloev na stali 20 s ispolzovaniem plazmennogo nagreva. *Svarochnoe proizvodstvo, 11*, 15-17.

Stalinskij, D.V., & Rudyuk, A.S. (2007). Sferidizaciya karbidnoj fazy v zaevtektoidnoj stali i ee vliyanie na svojstva relsov. *Metallurgicheskaya i gornorudnaya promyshlennost, 2*, 48-54.

Suhomlin, G.D. (1974). Elektronno-difrakcionnoe issledovanie orientacionnyh sootnoshenij ferrit-cementit v perlite. *FMM*, *38*(4), 878-880.

Tabieva, E.E., Popova, N.A., Nikonenko, E.L., Uazyrkhanova, G.K., & Gromov, V.E. (2020). Influence of surface quenching on morphology and phase composition of ferritic-pearlitic steel. *Izvestiya Ferrous Metallurgy, 63*(11-12), 915–921.

Tabieva, E.E., Rahadilov, B.K., Uazyrhanova, G.K., & Bajzhan, D. (2020). Struktura i mehanicheskie svojstva kolesnoj stali do i posle elektrolitno-plazmennoj poverhnostnoj zakalki. *Vestnik VKTU, 3*.

Tabieva, E.E., Uazyrhanova, G.K., Popova, N.A., & Nikonenko E.L. (2020). Vliyanie poverhnostnoj zakalki na izmenenie strukturno-fazovogo sostoyaniya st2. *Fundamentalnye problemy sovremennogo materialovedeniya, 2*, 169-175.

Tabiyeva, E., Rahadilov, B., Uazyrkhanova, G., Satbaeva, Z., & Kengesbekov A. (2019). Influence of electrolytic-plasma surface hardening on the surface properties of bandage steel. *TRIBOLOGIA, 4*, 105-111.

Tabiyeva, Y. Y., Popova, N. A., & Nikonenko, E. L. (2020). Influence of electrolytic-plasma treatment on the morphological components of the matrix of steels of ferrite-perlite class. *International Scientific and Technical Conference PRFN-2020*. Tomsk.

Tabiyeva, Y. Y., Rakhadilov, B. K., Uazyrkhanova, G. K., Zhurerova, L. G., Sagdoldina, Zh. B., & Kurbanbekov, S. K. (2019). *Research of change in tribological properties of steel grade two after electrolytic-plasma exposure*. 11th International Scientific Conference "Chaos and Structures in Nonlinear Systems, Karaganda..

Troyannikov, A.Y. (2021). Sravnitelnyj analiz vysokoenergeticheskih metodov poverhnostnogo uprochneniya stali. *Molodoj uchenyj, 19,* (361).

Tyuftyaev, A.C. (2002). *Zakonomernosti strukturoobrazovaniya pri plazmennoj obrabotke stali 60 G i promyshlennoe osvoenie tehnologii poverhnostnogo uprochneniya grebnej zheleznodorozhnyh kolesnyh par.* OIVTRAN.

Tyuftyaev, A. S. (2002). *Zakonomernosti strukturoobrazovaniya pri plazmennoj obrabotke stali 60G i promyshlennoe osvoenie tehnologii poverhnostnogo uprochneniya grebnej zheleznodorozhnyh kolesnyh par*. FGUP CNIIchermet im. I.P.Bardina. Moskva.

Tyuirin, Y.N. & Pogrebnjak, A.D. (2001). *Electric Heating Using a Liquid Electrode*, 142-144. Surf. And Coat. Tech.

Tyurin, Y. (1999). *Technology and equipment electrolytic-plasma quenching*. 3rd Intern. conf. on quenching and control of distortion. Prague.

Tyurin, Y. (2000). Features and advantages of surface modification of metallic pieces using electrolytic plasma thermal cycling hardening. *Plasma Surface Eng*, 1230-1233.

Tyurin, Y.I. (1999). *Osobennosti elektrolitno-plazmennoj zakalki. 3-ya mezhdunarodnaya konferenciya. Vzaimodejstvie izluchenij s tverdym telom*. Minsk.

Uazyrkhanova, G. K., Rakhadilov, B. K., Tabieva, E. E., & Baizhan, D. (2020). The influence of electrolyte-plasma surface hardening on the strength characteristics of grade two steel. *VI International Scientific and Practical Conference "Science and education in the modern world: challenges of the XXI century".* Nur-Sultan.

Utevskij, L.M. (1973). *Difrakcionnaya elektronnaya mikroskopiya v metallovedenii*. Metallurgiya.

Van Gyui, V. (2015). Plazmennaya cementaciya uglerodistyh stalej s ispolzovaniem past v tverdoj faze. *Vestnik nauki i obrazovaniya Severo-Zapada Rossii, 1*, 205-211.

Van Gyui, V. (2015). Parovodyanaya plazmennaya cementaciya v tverdoj faze na ustanovke MULTIPLAZ 3500. *Innovacii v nauke, 51* (1), 95-102.

Vyacheslav, F.B. & Szczerek, M. (2018). The influence of surface layer quality on the performance characteristics of machine parts under machining. *Tribologia, 271*(1), 23-29.

Wang, B., Jin, X., Xue, W., Wu, Z., Du, J., & Wu. J. (2013). High temperature tribological behaviors of plasma electrolytic borocarburized Q235 low-carbon steel. *Surface & Coatings Technology, 232*, 142-149.

Weinberg, F. (1973). *Pribory i metody fizicheskogo metallovedeniya*, *1*.

Yerokhin, A.L., Nie, X., Leyland, A., Matthews, A., & Dowey S.J. (1999). Plasma electrolysis for surface engineering. *Surface and Coatings Technology, 122*, 73-93.

Yushenko, K.A., Borisov, Y.S., & Tyurin, Y.N. (1994). *Teoriya i praktika impulsno-plazmennogo modificirovaniya poverhnosti detalej mashin i instrumenta.* Svarochnoe proizvodstvo. Kiev.

Zaides S.A., Van Huy, V., & Van, D. (2020). Developing installation to increase cylindrical part surface hardness. *Proceedings of Irkutsk State Technical University, 24*(2), 262-274.

Zhang P., Nie X., & Northwood D.O. (2009). Influence of coating thickness on the galvanic corrosion properties of Mg oxide in an engine coolant. *Surface & Coatings Technology, 203*, 3271-3277.

Zhang, W. (2002). Integrated modeling of thermal cycles, austenite formation, grain growth and decomposition in the heat affected zone of carbon steel. *Science and Technology of Welding and Joining, 5*, 574-582.

Zhang W. (2002). Kinetics of Ferrite to Austenite Phase Transformation during Welding of 1005 Steel. *Scripta Materialia, 46*, 753-757.

Zhang, W. (2002). Modeling and Real Time Mapping of Phases during GTA Welding of 1005 Steel. *Materials Science and Engineering A, 333,* 320-335.

Zhang W., Elmer J.W., & Debroy T. (2005). Integrated modeling of thermal cycles, austenite formation, grain growth and decomposition in the heat affected zone of carbon steel. *Science and Technology of Welding and Joining, 10* (5), 574-582.